Sabiu Said ABDULLAHI

SYNTHESIS AND CHARACTERIZATION OF Mn AND Co CODOPED ZnO ($Mn_xCo_{0.1}Zn_{0.9-x}O$) NANOPARTICLES

2014

FATİH UNIVERSITY

The Graduate School of Sciences and Engineering

Master of Science in
Physics

SYNTHESIS AND CHARACTERIZATION OF Mn And Co CODOPED ZnO ($Mn_xCo_{0.1}Zn_{0.9-x}O$) NANOPARTICLES

by

Sabiu Said ABDULLAHI
January 2014.

SYNTHESIS AND CHARACTERIZATION OF Mn AND Co CODOPED ZnO ($Mn_XCo_{0.1}Zn_{0.9-X}O$) NANOPARTICLES

by

Sabiu Said ABDULLAHI

A thesis Submitted to

The Graduate School of Sciences and Engineering

of

Fatih University

in Partial fulfillment of the Requirements for the Degree of

Master of Science

in

Physics

January, 2014
Istanbul, Turkey

APPROVAL PAGE

This is to certify that I have read this thesis written by Sabiu Said Abdullahi and that in my opinion it is fully adequate, in scope and quality, as a thesis for the degree of Master of Science in Physics.

_____
Prof. Dr. Yüksel KÖSEOĞLU
Thesis Supervisor

_____
Assoc. Prof. Dr Sadik GÜNER
Co-Supervisor

I certify that this thesis satisfies all the requirements as a thesis for the degree of Master of Science in Physics.

_____
Prof. Dr. Mustafa KUMRU
Head of Department

Examining Committee Members

Prof. Dr. Yüksel KÖSEOĞLU _____

Assoc. Prof. Dr Sadık GÜNER _____

Assoc. Prof. Dr. Serkan ÇALIŞKAN _____

Assoc. Prof. Dr. Ramazan ÖZTÜRK _____

Assoc. Prof. Dr. Ahmet ALTUN _____

It is approved that this thesis has been written in compliance with the formatting rules laid down by the Graduate School of Sciences and Engineering.

_____
Assoc. Prof. Dr. Nurullah ARSLAN
Director

January 2014.

SYNTHESIS AND CHARACTERIZATION OF Mn AND Co CODOPED ZnO ($Mn_XCo_{0.1}Zn_{0.9-X}O$) NANOPARTICLES

Sabiu Said ABDULLAHI

M.S. Thesis – Physics
January 2014

Supervisor: Prof. Yüksel KÖSEOĞLU

Co-supervisor: Assoc. Prof. Dr. Sadik GÜNER

ABSTRACT

$Mn_xCo_{0.1}Zn_{0.9-x}O$ nanoparticles with different doping concentration (x=0.0, 0.05, 0.1, 0.15, 0.2) has been successfully synthesized by microwave assisted combustion synthesis method using urea as a fuel. The structural, morphological compositional, magnetic and optical properties of these nanoparticles were investigated by X-ray diffraction (XRD), Scanning electron microscopes (FE-SEM JEOL-7001), Energy-dispersive X-ray spectroscopy (EDX), Quantum design Physical Property Measurement System (PPMS) and UV-Visible spectroscopy respectively. The structural properties showed the formation of single phase Wurtzite structure of ZnO without any indication of secondary phase, the average size of the nanoparticles was estimated using Debye- Scherrer's equation which lies between 32.65-23.69nm , It suggests the prevention of crystal growth as a result of Mn^{2+} doping in ZnO. The Scanning electron microscopy reveals that the samples consist of almost spherical shaped nanoparticles and no any indication of phase separation and agglomeration. A close view of particles also shows that smaller crystallites have sizes smaller than 100 nm. Similarly Energy-dispersive X-ray spectroscopy (EDX) confirms that the chemical composition tallies with the synthesis results. The magnetic characterization of the samples reveals that the sample shows paramagnetic and Ferromagnetic behavior the paramagnetic behavior can be attributed to the incorporation of Mn ions in ZnO structure, mean while there is no linear variation of magnetic moment with Concentration of Mn ion whereby at x=0.15 the samples show Ferromagnetic behavior with coercive field and remanent magnetization of 47.70Oe and $1.8x10^{-1}$ (emu/g) respectively. Similarly the possibility for the room temperature ferromagnetic contribution is presence in 0.2 sample is

observed from the temperature dependent magnetization curves, during zero field cooling (ZFC) and field cooling (FC) in an applied magnetic field of 500Oe, moreover the optical band gap varies between3.24 eV and 3.02 eV.

Keywords: Magnetic Nanoparticles, Mn Co, ZnO, XRD, SEM, EDX, VSM, UV-Vis, Paramagnetic Ferromagnetic.

Mn ve Co Birlikte Katkılanmış ZnO Nanoparçacıkların Sentezi ve Karakterizasyonu

Sabiu Said Abdullahi

Yüksek Lisans Tezi – Fizik
Ocak 2014

Danışman: Prof. Yüksel KÖSEOĞLU

Eş Danışman: Doç. Dr. Sadik Güner

ÖZ

Bu çalışmada, $Mn_xCo_{0.1}Zn_{0.9-x}O$ nanoparçacıklar yakıt olarak üre kullanılarak, mikrodalga destekli yanma sentez metodu ile farklı katkı konsantrasyonlarda (x=0.0, 0.05, 0.1, 0.15, 0.2) başarılı bir şekilde sentezlenmiştir. Bu nanoparçacıkların yapısal, morfolojik, bileşimsel, manyetik ve optik özellikleri sırasıyla X-ışını kırınım cihazı (XRD), taramalı elektron mikroskobu (FE-SEM JEOL-7001), enerji dağılımlı X-ışını kırınım cihazı (EDX), kuantum tasarım fiziksel özellik ölçüm sistemi (PPMS) ve UV-görünür spektroskopisi kullanılarak incelendi. Yapısal özellikler tek fazlı ZnO Wurtzite yapısının oluşumunu, ikincil fazın hiçbir belirtisi olmadan gösterdi, nanoparçacıkların ortalama boyutları Debye-Scherrer's denklemi kullanılarak 32.65-23.69 nm olan değerler arasında hesaplandı. Bu, ZnO içindeki Mn^{2+} katkısı sonucu oluşan kristal büyümenin engellendiğini göstermektedir. Taramalı elektron mikroskobu örneklerin neredeyse hepsinin küre şeklindeki nanoparçacıklar olduğunu herhangi bir faz ayrımı ve yığıntı belirtisi göstermeden ortaya çıkardı. Parçacıklara yakın bir bakış açısı ayrıca daha küçük kristalitlerin boyutlarının 100 nm'den küçük olduğunu gösterir. Aynı şekilde enerji dağılımlı X-ışını kırınımı (EDX) kimyasal bileşim çetelesini sentez sonuçlarını seğirdiğini doğrular.Örneklerin manyetik karakterizasyonu; örneklerin paramanyetik ve ferromanyetik davranış gösterdiğini ortaya çıkarır ve paramanyetik davranış ZnO yapısındaki Mn iyonlarına atfedilebilir, buda Mn iyonlarının konsantrayonuyla manyetik momentin hiçbir doğrusal varyasyonu olmadığını, x=0.15 de örneklerin zorlayıcı alan ve sırasıyla 47.70 Oe ve $1.8x10^{-1}$ (emu/g) mıknatıslanma ile ferromenyetik davranış göstermesi vasıtasıyla anlşılır.Benzerbir şekilde0.2 örneği içindeki oda sıcaklığında ferromanyetik katılımın varlığı 500 Oe'lik bir manyetik alanda sıfır alan soğutma (ZFC) ve alan soğutma (FC) sırasında sıcaklığa bağlı mıknatıslanma eğrilerinden gözlemlenmiştir, dahası optiksel bant genişliği 3.24 eV ve 3.02 eV arasında

değişir. Katkılanan Mn^{2+}iyonları örneklerin optiksel özellikleri üzerinde önemli bir etkiye sahip olduqu bulunmuştur.

Anahtar Kelimeler: Manyetik nanoparçacıklar, Mn, Co, ZnO, XRD, SEM, EDX, VSM, UV-Vis., Paramanyetik, Ferromanyetik.

To my family

ACKNOWLEDGEMENT

All praise is due to Allah to whom all good deeds and favors comes from him. I would like to express my sincere gratitude to my supervisor Prof. Dr. Yüksel KÖSEOĞLU for his support, encouragement guidance and concern during the course of research and writing of this thesis.

My Special gratitude goes to my Co Supervisor Assoc. Prof. Dr Sadık GÜNER for his continuous support toward the completion of this thesis.

My thanks go to Prof. Dr. Mustafa KUMRU for his academic guidance throughout my Masters Degree Program.

I would like to thank Assist. Prof. Dr. Sinan KAZAN for magnetic measurements. I wish to thank my friends and Colleagues like, Osman,GURAVEN, Yasin Celaleddin, DURMAZ, Ismail KURT, Muhammed Rıza AKYÜZ, Shamsu AHMAD, Yusuf SHEHU, Haidar MASUD and Muttaqa Uba ZANGO, for their encouragement, advice and valuable help during the research and writing this thesis.

Moreover I will like to convey my gratitude to Kano State Government Under the tenure ship of Dr. Rabiu Musa KWANKWASO for awarding me with the scholarship throughout my Masters Degree program

Finally my regard and appreciation to Fatih University especially to Physics Department for providing me with good atmospheric condition for learning including research facilities with professional and outstanding teachers.

TABLE OF CONTENTS

LIST OF TABLES

TABLE

LIST OF FIGURES

FIGURE

LIST OF SYMBOLS/ABBREVIATIONS

SYMBOL/ABBREVIATION

SEM	Scanning Electron Microscopy
DMS	Dilute Magnetic Semiconductor
eV	Electron Volt
UV	Ultra Violet
LED	Light Emitting Diodes
OLEDs	Organic Light Emitting Diodes
TFT	Transparent Thin Films Transistors
LTPS	Low-Temperature Poly-Si
LCD	Liquid Crystal Display Panels
BEs	Bound Excitons
DBE	Donor Bound Exciton
ABEs	Acceptor-Bound Excitons
TM	Transition Metal
RTFM	Room-Temperature Ferromagnetism
FET	Field Effect Transistor
me	Free-Electron Mass
T_C	Curie Temperature
M	Magnetization
H	Magnetic Field
T	Temperature
K	Kelvin
Θ_0	Curie-Weiss Temperature
C_0	Curie Constant
B	Bohr Magneton
K_B	Boltzman Constant
B	External Magnetic Field

N_0	Density
$B_{5/2}$	Brillioun Function
S_{sat}	Saturation Value
T_{eff}	Rescaled Temperature
q	Charge
χ_m	Susceptibility
μ_0	Permeability of Free Space
μ	Permeability
XRD	X- ray Diffraction Technique
D	Crystalline Size
B	Full Width of the Half Maximum of the Most Intense Peak
FWHM	Full width of the half maximum
λ	Wavelength
θ	Bragg angle
d	Lattice Spacing
a and c	Lattice Constants
hkl	Miller Indices
EDX	Energy Dispersive X-ray Spectroscopy
PPMS	Physical Property Measurement System
VSM	Vibrating Sample Magnetometers
DC	Direct Current
VIS	Visible
IR	Infra Red
DR	Diffuse Reflection
K	Absorption Coefficient
E_g	Energy Band Gap
R_∞	Limiting Reflectance
$F(R_\infty)$	Kubelka-Munk Function
α	Linear Absorption Coefficient
υ	Light Frequency
A	Proportionality constant
FE-SEM	Field effect Scanning Electron Microscopes
FC	Field Cooling

ZFC	Zero Field Cooling
RT	Room Temperature

CHAPTER 1

INTRODUCTION

1.1 GENERAL INTRODUCTION

The progress of technology and quality of life of mankind has always been improved with the advancement in material science and technology. Most material processing techniques are based on breaking up larger scale materials into desired shapes and sizes, inducing strain, lattice defects and other deformations in the processed materials [1]. Recent developments in nanotechnology and the demonstration of various quantum size effects in nanoscale particles implies that most of the novel devices of the future will be based on properties of nanomaterials.

Nanotechnology today is growing very rapidly and has infinite applications in almost everything we do. The medicine we take, food we eat, chemicals we use, car we drive and much more in our life endeavor [2]. Because of that, nanotechnology research has gained power in the recent years by creating solutions in the field of biomedical, materials science, optics and electronics etc. As such, nanotechnology is a science, engineering, and technology conducted at the nanoscale, which is about 1 to 100 nanometers [3].

The ideas and concepts behind nanoscience and nanotechnology started with a talk entitled " There's plenty of room at the bottom'' by physicist Richard Feynman at an American Physical Society meeting at the California Institute of Technology (CalTech) on December 29, 1959, before then the term nanotechnology was used. In his talk, Feynman described a process in which scientists would be able to manipulate and control individual atoms and molecules. Over a decade later, in his explorations of ultra-

precision machining, Professor Norio Taniguchi coined the term nanotechnology. It wasn't until 1981, with the development of the scanning tunneling microscope (SEM) that could see individual atoms, [3] that modern technology began.

Although modern nanoscience and nanotechnology are quite new, nanoscale materials were used since before, where alternate-sized gold and silver particles created colors in the stained glass windows of medieval mosques and churches hundreds of years ago. The artists back then just didn't know that the process they used to create these beautiful works of art actually led to changes in the composition of the materials they were working with [3].

Today's scientists and engineers are finding a wide variety of ways to intentionally make materials at the nanoscale to take advantage of their enhanced properties such as higher strength, lighter weight, increased control of light spectrum, better physical properties and greater chemical reactivity than their larger-scale counterparts. Therefore it is possible to arrange atoms into structures that are only a few nanometers in size. A particularly attractive goal is the self-assembly of nanostructures, which produces large amounts of artificial materials with new properties [3]. In order to connect nanostructures to the more familiar world of microstructures and microelectronics, one wants to build up larger assemblies by guided self-assembly. However here we are going to discuss more on magnetic nanostructure.

Magnetic nanomaterials have gained great interest of scientists due to their unusual physical properties compared to their bulk counterparts. They have very large area of application in technology, such as electronic devices, microwave devices, transformer cores, magnetic devices, switching devices, recording tapes, permanent magnets, hard disc recording media, flexible recording media, magnetic drug delivery catalysis, color imaging, magnetic refrigerator, detoxification of biological fluids, etc [4]. Especially magnetic diluted semiconducting (DMS) nanoparticles due to their broad applications [5] in different important technological fields, such as spintronics, magnetic semiconductors, catalysts, sensors, field emission devices, solar cells [6] etc.

Among these semiconducting materials, ZnO is a semiconducting material with a wide energy band gap of 3.37 eV and large exciting binding energy of approximately 60 meV at 300 K [5]. It is widely studied material where by great attention is focused on

because of its ferromagnetic behaviour at room temperature when doped with transtion metals such as Fe, Co, Cu, Mn, etc. Moreover, it can be used in many areas unlike most of the materials with which it competes, ZnO is inexpensive, relatively abundant, chemically stable, easy to prepare and non-toxic. Similarly, most of the doping materials that are used with ZnO are readily available [7].

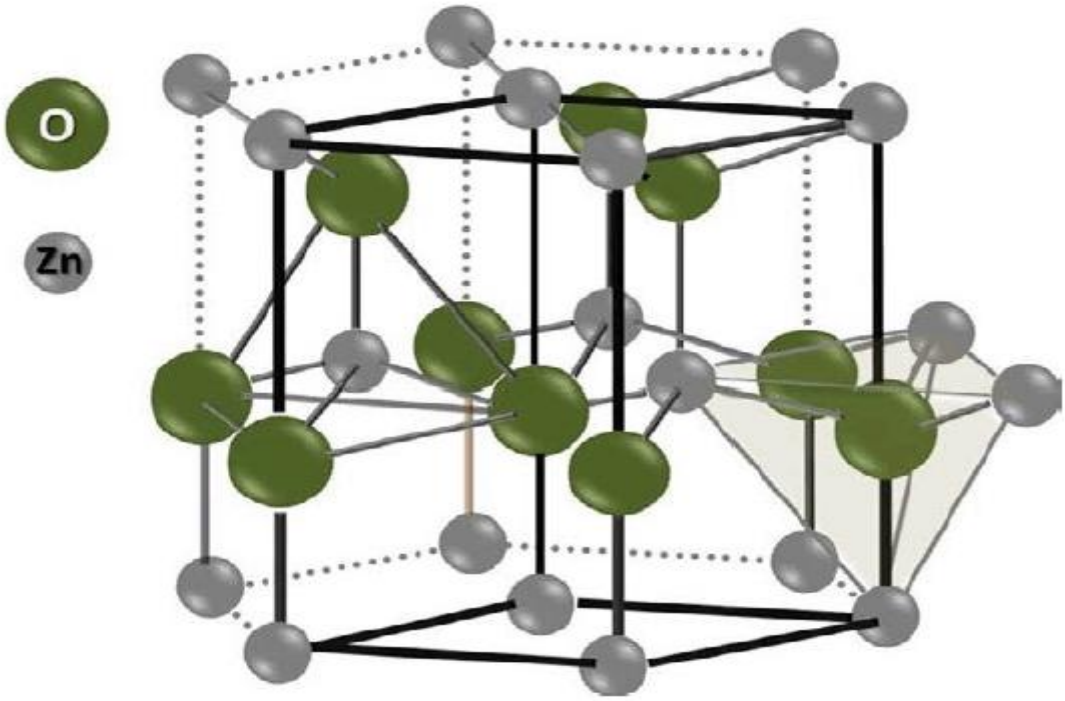

Figure 1.1 Crystalline Wurtzite Structure Model of ZnO

1.2 THE CRYSTAL AND SURFACE STRUCTURE OF ZnO

Generally, zinc oxide has a Wurtzite hexagonal structure (space group P63*mc*) with lattice parameters a = 0.3296nm and c = 0.52065 nm. The structure of ZnO can be simply described as a number of alternating planes composed of tetrahedrally coordinated O^{2-} and Zn^{2+} ions, stacked alternately along the *c*-axis (see figure1.1). The tetrahedral coordination in ZnO results in non central symmetric structure and consequently piezoelectricity and pyroelectricity [8]. Another important characteristic of ZnO is polar surfaces. The most common polar surface is the basal plane. The oppositely charged ions produce positively charged Zn-(0001) and negatively charged O-$(000\bar{1})$ surfaces, resulting in a normal dipole moment and spontaneous polarization

along the *c*-axis as well as a divergence in surface energy. To maintain a stable structure, the polar surfaces generally have facets or exhibit massive surface reconstructions, but ZnO ±*(*0001*)* are exceptions: they are atomically flat, stable and without reconstruction [8]. Efforts to understand the superior stability of the ZnO ±*(*0001*)* polar surfaces are at the forefront of research in today's surface physics. The other two most commonly observed facets for ZnO are $\{2\bar{1}\bar{1}0\}$ and $\{01\bar{1}0\}$, which are non-polar surfaces and have lower energy than the {0001} facets.

1.3 PROPERTIES OF ZINC OXIDE

1.3.1 Physical and Optical Properties of Zinc Oxide

ZnO is a high carrier mobility semiconducting materials which is directly linked to its transparency, this makes it fully possible for ZnO to compete with existing silicon materials. Moreover the wide band gap of ZnO is important because it opens the possibility of creating Ultra Violet (UV) light emitting diodes (LEDs) and white LEDs with superior color purity. In addition to that ZnO is Low temperature processing compound which is preferred in some applications such as organic light emitting diodes (OLEDs) [9].due to its being as transparent semiconductors there has been a sharp jump in its need for higher carrier mobility of transparent semiconductors. The carrier mobility determines transparent thin films transistors (TFT) characteristics. This is now exceeding the carrier mobility of materials such as low-temperature poly-Si (LTPS) and amorphous Si used in liquid crystal display (LCD) panels.

1.3.2 Optical Properties of ZnO

The optical properties of a semiconductor are connected with both intrinsic and extrinsic effects. Intrinsic optical transitions take place between the electrons in the conduction band and holes in the valence band, including excitonic effects due to the Coulomb interaction [10]. Excitons are classified into free and bound excitons. In high-quality samples with low impurity concentrations, the free exciton can also exhibit excited states, in addition to their ground-state transitions. Extrinsic properties are related to dopants or defects, which usually create discrete electronic states in the band

gap, and therefore influence both optical-absorption and emission processes. The electronic states of the bound excitons (BEs) depend strongly on the semiconductor materials [10]. in particular the band structure. In theory, excitons could be bound to neutral or charged donors and acceptors. A basic assumption in the description of the principal bound-exciton states for neutral donors and acceptors is a dominant coupling of the like particles in the bound exciton states. For a shallow neutral-donor bound exciton (DBE), for example, the two electrons in the BE state are assumed to pair off into a two-electron state with zero spin. The additional hole is then weakly bound in the net hole-attractive Coulomb potential set up by this bound two- electron aggregate. Similarly, shallow-neutral acceptor-bound excitons (ABEs) are expected to have a two hole state derived from the top most valence band and one electron interaction. These two classes of bound excitons are by far the most important cases. Other defect-related transitions could be seen in optical spectra such as free to bound electron-acceptors, bound to bound donor-acceptors, and the so-called yellow/green luminescence.

Moreover Optical transitions in ZnO have been studied by a variety of experimental techniques such as optical absorption, transmission, reflection, photo reflection, spectroscopic ellipsometry, photoluminescence, cathode luminescence, calorimetric spectroscopy, etc [11].

1.4 MAGNETIC PROPERTY

Many experiments have shown that it is possible to induce room-temperature ferromagnetic-like behavior in ZnO nanoparticles without doping with magnetic impurities but simply inducing an alteration of their electronic configuration. Capping ZnO nanoparticles (~10 nm size) with different organic molecules produces an alteration of their electronic configuration that depends on the particular molecule, as evidenced by photoluminescence and X-ray absorption spectroscopic and altering their magnetic properties that varies from diamagnetic to ferromagnetic-like behavior [12].

1.5 ELECTRICAL PROPERTIES OF ZnO

The fundamental study of the electrical properties of ZnO nanostructures is vital for developing their future applications in nano electronics, As a direct and large-band-gap material [10].ZnO is attracting a lot of attention for a variety of electronic and optoelectronic applications. Moreover advantages associated with a large band gap include higher breakdown voltages, ability to sustain large electric fields, lower noise generation, high temperature and high-power operation. The electron transport in semiconductors can be considered for low and high electric fields. That is at sufficiently low electric fields, the energy gained by the electrons from the applied electric field is small compared to the thermal energy of electrons, and therefore, the energy distribution of electrons is unaffected by such a low electric Field [11]. Since the scattering rates determining the electron mobility depend on the electron distribution function, electron mobility remains independent of the applied electric field, and Ohm's law is obeyed. On the other hands when the electric field is increased to a point where the energy gained by electrons from the external field is no longer negligible compared to the thermal energy of the electron, the electron distribution function changes significantly from its equilibrium value. These electrons become hot electrons characterized by an electron temperature larger than the lattice temperature. Furthermore, as the dimensions of the device are decreased to submicron range, transient transport occurs when there is minimal or no energy loss to the lattice during a short and critical period of time, such as during transport under the gate of a field-effect transistor or through the base of a bipolar transistor [11]. The transient transport is characterized by the onset of ballistic or velocity overshoot phenomenon. Since the electron drift velocity is higher than its steady-state value, one can design a device operating at frequencies exceeding those expected from linear scaling of dimensions.

1.6 DOPING OF ZnO

ZnO because of its being highly regarded as a material with strong potential for various short-wavelength optoelectronic device applications. Therefore to attain the potential offered by ZnO, both high-quality *n*- and *p*-type ZnO are unavoidable [13], However, difficulty in bipolar carrier doping, that is both *n* and *p* types is a major

obstacle as seen in other wide-band-gap semiconductors such as GaN and II-VI compound semiconductors including ZnS, ZnSe, and ZnTe. Unipolar doping has not been a surprising issue in wide-band-gap semiconductors: ZnO, GaN, ZnS, and ZnSe are easily doped to *n*-type, while *p*-type doping is difficult. The situation is opposite for ZnTe where *p*-type doping is easily obtained, while *n*-type doping is difficult [10].

Recently transition metal (TM) doped ZnO diluted magnetic semiconductors (DMSs) have attracted much scientific interest because, their potential as both charge and spin degrees of freedom can be manipulated by replacing a small fraction of nonmagnetic host semiconductor atoms by magnetic ions. These types of material are potential candidates for technological applications in optoelectronics, magnetoelectronics, spintronics and microwave devices. From a feasible application point of view, a key requirement is that the material be ferromagnetic at or above room temperature [13]. Similarly the theoretical prediction of room temperature and above ferromagnetism TM doped ZnO-based DMSs for spintronics applications [14]. This prediction motivated many experimental studies on DMS particles by using different synthesis methods and they addressed the magnetic properties for TM doped ZnO DMSs measured by various methods [15].

A number of studies indicate that the room-temperature ferromagnetism in these materials might come from precipitation of magnetic clusters or secondary magnetic phases [16]. However, there are different studies indicating the absence of magnetic clusters, secondary phases or impurities and support intrinsic ferromagnetic origin [17]. Although there have been many experimental results, there has not been a consensus on the origin of ferromagnetism and physics underlying this magnetic behavior of TM doped oxides. These controversial results show that the magnetism of DMSs is sensitive to preparation methods and conditions. Furthermore, even magnetic properties of DMSs prepared by the same method for the same doping concentration show the lack of reproducibility [18]. Also, there is not a physical theory as yet, able to explain the differences in magnetic properties and conflicting reports [13]. Moreover, for solid state light emitting diodes, photonics and also in data storage systems transition metal ions doped zinc oxide systems are also applicable [1].

There is a great enhancement of atomic spin effect when transitional metallic elements such as Fe, Co, Ni and Mn along with some rare earth elements are present in

oxide systems and this enhancement may be due to the cooperative interactions of large number of these atomic spins producing a region where all atomic spins within it are aligned parallel [1]. Among all transition metals doped ZnO system, Co-doped ZnO has attracted considerable interest [1, 19]. Due to a number of reports about the observation of room-temperature ferromagnetism (RTFM) in its powder (Zn1-xCoxO) [13].that is why tremendous theoretical and experimental works focused on the Co-doped ZnO as DMS. Therefore, it is important to know the structural characteristics, electrical and optical properties of these materials. Although changing of these properties depending on the doping has been widely studied, however Research are still ongoing.

.

1.7 ZNO-BASED DILUTE MAGNETIC SEMICONDUCTORS

Metal Oxide diluted magnetic semiconductors (DMSs) have attracted considerable attention because the spin-dependent magnetic phenomena can be manipulated [20]. Generally, 3*d* transition-metal ions are substituted for the cations of the host semiconductors [10]. Because of that the electronic structure of the substituted 3*d* transition-metal impurities in semiconductors is influenced by two competing factors: strong 3*d*-host hybridization and strong Coulomb interactions between 3*d*-3*d* electrons [10]. The latter is responsible for the multiplet structures observed in *d*-*d* optical-absorption spectra. On the other hand, as specifically shown for the Mn-doped systems the hybridization between the transition-metal 3*d* and the host valence band gives rise to the magnetic interaction between the localized 3*d* spins and the carriers in the host valence band. With the significant advance of the materials engineering of thin-film and nanoscale heterostructures, the quantized energy levels in semiconductor nanostructures can be coupled either with local magnetic fields created by integrated submicron ferromagnetic structures or with the exchange fields of magnetic ions into the semiconductor lattice itself [7], hence providing a foundation for quantum spin devices including single-electron spin transistors that rely on spin-dependent tunneling into a magnetic quantum dot and magnetic field-effect transistor that employ injection of spin polarized carriers into transport channels.

The observation of ferromagnetic transitions in III-V and II-VI type semiconductors at high temperature (Curie temperature 100K) has recently attracted a

great deal of attention. Demonstration of long spin-coherence time in semiconductors and rapid development of the information storage technology using ferromagnetic metals have heightened the research activities in this field. As semiconductors have many potential advantages over metals [10], because they can be easily change to form an appropriate heterostructure with impurities, the actual fabrication of ferromagnetic semiconductors that work at room temperature remains very attractive for the device applications. The recent discussion of ferromagnetism though controversial at temperatures much higher than the room temperature in MnZnO, CoZnO, has gives hope that these materials will indeed have profound technological impact [21]. If accomplished, above room-temperature ferromagnetism could form the basis for charge, spin-based, or mixed spin- and charge-based devices. The devices utilizing spin in one form or another fall into a newly coined nomenclature spintronics. Spintronics is a paradigm in which the spin degree of freedom of the electron is harnessed either by exploiting the spin property in conventional charge-based devices or utilizing the spin alone. For successful incorporation of spin into existing semiconductor technology several technical issues such as efficient injection, transport, manipulation, and detection of spin polarization as well as spin polarized currents must be resolved. Faster and less-power consuming transistors could be achieved since flipping the spin takes 10–50 times less power and is ten times faster than transporting an electron through the channel in traditional FETs. Potential applications for ferromagnetic semiconductors and oxides include electrically controlled magnetic sensors and actuators, high-density ultralow-power memory and logic, spin-polarized light emitters for optical encoding, advanced optical switches and modulators, and devices with integrated magnetic, electronic, and optical functionality. Challenges are formidable in that in addition to coherent spin injection, the device dimensions must be comparable if not less than the spin-coherence lengths.[10]

Since ZnO can be made ferromagnetic by doping with transition metals such as Mn, Fe, Cr, Co, [22] etc., or when spin injecting contacts to ZnO can be found, the material would be suitable for spin FETs. In ZnO, the equilibrium solubility limit of 3*d* transition metals such as Mn is larger than 10 mol %, and the electron effective mass is as large as 0.3*me,* where *me* is free-electron mass. Therefore the amount of injected spins and carriers in the ZnO can be large, thus making Mn-doped ZnO ideal for the fabrication of spintronic devices. If it is made as ferromagnetic, it can be used for drain

and source in FET. Several groups have fabricated TMZnO, where TM=, Mn, Fe, Co, Ni, Cu and films by different techniques [10, 13, 19, 20]. Interestingly, several quantum structures derived from the ZnO-based DMS (particularly, substituting Zn site by Mn) provide a valuable framework for understanding of spin transport and dynamics in magnetically active quantum semiconductor structures,

1.9 THEORY OF ZnO-BASED MAGNETIC SEMICONDUCTORS

There are two basic approaches in understanding the magnetic properties of dilute magnetic semiconductors. The first group of approaches, which are based on the general mean-field theory, implicitly assumes that the dilute magnetic semiconductor is a more-or-less random alloy, e.g., TMZnO, in which transition-metal (TM) substitutes for one of the lattice constituents. The ferromagnetism occurs through interactions between the local moments of the TM atoms, which are mediated by free carriers in the material [10]. The spin spin coupling is also assumed to be a long-range interaction, allowing use of a mean-field approximation. Virtual crystal approximation is used to calculate the effective spin density due to the TM-ion distribution. The direct TM-TM interactions are antiferromagnetic so that the Curie temperature T_C for a given material with a specific TM concentration and hole density is determined by a competition between the ferromagnetic and antiferromagnetic interactions. The second group of approaches suggests that the magnetic atoms form clusters that produce the observed ferromagnetism. Principally, the majority of DMS studied in an extensive way until now involved Mn^{2+} ion as a legitimate member of the transition-metal family to be embedded in various II-VI and III-V hosts. The easy substitution of Mn for the group-II elements in both zinc-blende and wurtzite structures occurs mainly due to the fact that the 3*d* orbitals of Mn^{2+} are exactly half-filled. As a result, all five spins are parallel in this orbital by Hund's rule and that will cost a considerable energy to add an electron with opposite spin to the atom, resulting in a complete 3d5 orbit. Therefore, Mn^{2+} has a relatively large magnetic moment (spin S=5/2 and angular momentum L=0) with characteristic of a half-filled d shell and can be incorporated in sizable amounts (up to 35% of Mn) into ZnO host without affecting much the crystallographic quality of the DMS, whereas about 5% is tolerable for III-V-based hosts. Additionally, Mn^{2+} is electrically neutral in II-VI hosts acting as neither acceptor nor donor, while it acts as an

acceptor in the III-V-based DMS. In view of this, Mn atom resembles a group-II element, hence has attracted many researchers to produce these materials using bulk growth techniques. . One may employ the band-gap engineering techniques to create new DMS materials by manipulating the various physical parameters involved. Apart from this, the presence of local moments allows the spin engineering of phenomena through the exploitation of two classes of exchange interactions. The first one is the *d-d* super exchange between *d* electrons of the magnetic ions, and the second one is the *sp-d* exchange between the *d* electrons and the band electrons or holes. This interaction is ferromagnetic for conduction-band states and mainly antiferromagnetic for valence bands. This interaction determines the spin splitting of the band states in an external magnetic field, giving rise to interesting magneto-optical and magneto transport responses in the DMS samples. To obtain the Curie temperature from the magnetic measurements, the Curie-Weiss law is used:

$$\frac{M}{H} = \frac{Co}{T-\theta o} \tag{1.1}$$

where *M* is the magnetization, *H* is the magnetic field, *T* is the temperature, X is the transition-metal composition, and Θ_0 and C_0 are the Curie-Weiss temperature and the Curie constant for *X*=1, respectively. The Curie constant may be expressed as [23].

$$Co = \frac{(g\mu_B)2}{3k_B} s(s+1)n = C_M \frac{\rho}{\mu} \tag{1.2}$$

where *g* is the intrinsic Lande *g* factor, *n* is the number of cation sites per unit volume, C_M is the Curie constant for *x* =1, ρ is the mass density, μ is the molar mass, *S* is the effective spin per transition-metal ion (*S*=3/2 for Mn2+), *B* is the Bohr magneton, and K_B is the Boltzman constant. Using (1) and (2) one can estimate Θ_0 and C_M. The effective exchange integral between the nearest-neighbor transition ions can be estimated from

$$\frac{J}{K_B} = \frac{3\theta_o}{3zs(s+1)} \tag{1.3}$$

Where z is the number of nearest-neighbor cations (z=12 for the wurtzite structure). A negative value of J_1 indicates that the interactions between the magnetic ions are antiferromagnetic, suggesting that super exchange is likely the dominant mechanism. For an external magnetic field B applied along the z direction, the magnetization M_Z of a DMS alloy containing Mn^{2+} ions is empirically written

$$M_z = N_o(s_z) + N_o s_{sat} B_{5/2}(5\mu_B B/k_B T_{eff}) \quad (1.4)$$

Where N_0 is the density of Mn^{2+} ions and $B_{5/2}$ is the Brillouin function for S=5/2, S_{sat} is the saturation value for the spin of an individual Mn^{2+} ions (i.e., smaller than 5/2), and the rescaled temperature $T_{eff}=T+T_0$. Along with the distribution of magnetic ions on a DMS lattice, isolated spins, pairs of spins, and triplets are also distributed. Hence the magnetization is dominated by the paramagnetic response of isolated single spins, which are antiferromagnetically coupled. However, if we consider a DMS heterostructure, the ferromagnetic *s-d* exchange interaction between conduction electrons and local moments results in an enhanced electronic spin splitting [10].

So in this study we are trying to enhance the ferromagnetic ordering and better conductivity of CoZnO, by subtituting Zn with Mn as in the formula ($Mn_xCo_{0.1}Zn_{0.9-x}O$), [24,25,26] where by forming the kind of soft magnetic materials with low coercivity, high anisotropy and their magnetic, electrical as well as optical properties will increase.

Therefore the technological importance of MnCoZnO has motivated several studies on the synthesis as well as the physical properties of this material. The magnetic properties of MnCoZnO have been studied using methods such as combustion, sol-gel method [25, 26]; in addition, the variation in the magnetic properties of nanocrystalline MnCoZnO powders as a function of particle size has been investigated.

CHAPTER 2

THEORETICAL BACKGROUND

2.1 SEMICONDUCTORS

2.2 DEFINITION OF SEMICONDUCTORS

Generally materials can be classified as metals, semimetals, semiconductors and insulators depending on how their band structure is.

Semiconductors are categories of materials having conductivities between those of metals and insulators [27]. They are the foundation of modern solid electronic devices such as transistors, solar cells, light emitting diodes (LEDs) [28], quantum dots, digital and analog integrated circuits [20,29,26], etc.

2.21 Types of Semiconductors

Semiconductors are classified as either intrinsic or extrinsic semiconductors. An intrinsic semiconductor is a semiconductor material that is chemically pure having poor conductivity due to its equal number of negative carriers (electrons) and positive carriers (holes). A silicon crystal is different from an insulator because at any temperature above the absolute zero temperature, there is a finite probability that an electron in the lattice will be knocked loose from its position, leaving behind an electron deficiency called a "hole". If a voltage is applied, then both the electron and the hole can contribute to a small current flow [30]. ZnO is an example of this type [1,18].

On the other hand, an extrinsic semiconductor is an intrinsic semiconductor doped with a small amount of impurities which lead to the alteration of electrical properties of

the material and improves its conductivity [31]. Consequently, it is leading to n-type or p–type semiconductor [32].

Moreover, semiconductor nanoparticles received most of the scientists' attention due to their good physical and chemical properties with respect to their bulk ones. They possess many peculiar properties like ultrafast optical nonlinear response, photoelectric switch and piezoelectric properties [27] etc.

2.3 BAND GAP

The term "band gap" refers to the energy difference between the top of the valence band and the bottom of the conduction band. The electrons are able to jump from one band to another. In order for an electron to jump from a valence band to a conduction band, it requires a specific minimum amount of energy for the transition. Moreover, a wide band gap is one of the novel properties of semiconductor [34]. A diagram illustrating the band gap is shown in Figure 2.1.

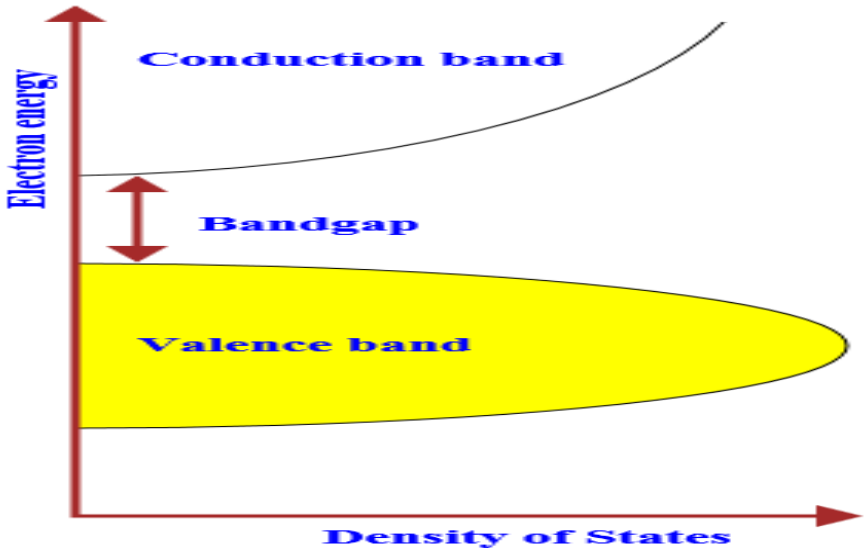

Figure 2.1 Energy band gap of a semiconductor.

Measuring the band gap is important for semiconductors and nanomaterial industries where by a wide band gap semiconductor is highly applicable [23]. The band gap energy of insulators is large (> 4eV), but lower for semiconductors (< 3eV) [35].
UV/Vis/NIR Spectrometer.

2.4 MAGNETISM AND MAGNETIC MATERIALS

In the fifth century B.C, the greeks were aware that certain natural rocks had an ability to attract each other as well attracts bits of iron. Because, these rocks where abundance near the ancient city of Magnesia, in the western city of Turkey and they become known as magnets [36]. So as Greeks of that time discovered the first naturally occurring magnetic stones, or natural magnets, observation of property of matter called magnetism starts to occur. Thus, magnetism is the force of attraction or repulsion in and around a material. Magnetism is present in all materials, but at such low levels that it is not easily detected. Certain materials such as magnetite, iron, steel, nickel, cobalt and alloys of rare earth elements, exhibit magnetism at levels that are easily be detected [37].

2.4.1 The Sources of Magnetism

The particles of a material as protons and neutrons are located inside the nucleus of an atom of the material, and the electrons are in constant motion around the nucleus. Electrons carry a negative electrical charge and produce a magnetic field as they move through space. A magnetic field is produced by an electrical charge in motion. The strength of this field is called the magnetic moment [38]. The source of magnetism lies in the orbital and spin motions of electrons and how the electrons interact with one another. To understand several types of magnetism one has to know how materials respond to an applied magnetic field as some materials are much more magnetic than others. The main distinction is that in some materials there is no collective interaction of atomic magnetic moments, where as in others there is a very strong interaction between atomic moments [39].

2.4.2 Magnetic Moment

The magnetic moment of a magnet is a quantity that determines the force that the magnet can exert on electric current and the torque that a magnetic field will exert on it. The expression for the magnetic moment is given below.

μ_t = IA (2.1)

and the torque is given by

$\tau = \mu_t$ x B (2.2)

The area around a magnet can also behave like a magnet. This is called a magnetic field.The larger the magnet and the closer the object to the magnet, the greater the force of the magnetic field.

2.5 MAGNETIC FIELD

When charge q is placed in an electric field it experience a force F even if the charge is not moving which is given by

F = qE (2.3)

But in the case of magnetic field the charge experience a force only if it is in motion so the magnetic force experience by charge q moving with a velocity v in a magnetic field B is given by

$$F = qv \times B \tag{2.4}$$

and the magnitude is given by

$$F = qvB\sin\theta \tag{2.5}$$

where θ is the angle of deviation and the direction of this force is perpendicular to that of v and B, therefore moving charge in the presence of a magnetic field experience a force and the converse is also true, that is to say moving charge or current create a magnetic field in the surrounding space which means that a conductor carrying an electric field is surrounded by a magnetic field. So the field lines due to a straight wire are circles concentric with the wire and the direction of the field can be predicted by right - hand rule [36].

The magnetization of a material can be given in terms of density of net magnetic dipole moment of the material [29]. Which is a vector quantity represented by M where

$$M = \mu_t / V \tag{2.6}$$

The source of the magnetic moment μ_t that cause the magnetization can be due to microscopic electric current resulting from the motion of electron in atoms or from either the spin of the electrons or the nuclei. Total magnetization results from the response of a material to an external magnetic field, together with any extra magnetic dipole moments that may be inherent in the material itself; Therefore the magnetization M is just the respond of the material to the magnetic field which is commonly defined by the equation

$$M = \chi_m H \tag{2.7}$$

where χ_m is the susceptibility of the material and H is the magnetic intensity measured in Amperes per meter, similarly H is given in terms of magnetic field B as

$$H = \frac{B}{\mu_0} - M \tag{2.8}$$

where μ_0 is the permeability of free space however for ferromagnetic materials with large magnetic susceptibility the permeability μ depends on the field and the magnetic state of the sample given as

$$B = \mu H \quad (2.9)$$

From the above equations it follows that

$$\mu = \mu_0(1+ \chi_m) \quad (2.11)$$

in the presence of an externally applied magnetic field $B_0$the net magnetization is given by

$$B = B_0 + \mu_0 M \quad (2.12)$$

2.6 MAGNETIC MATERIALS

The magnetic behavior of materials can be classified into the following five major groups:

1. Diamagnetism
2. Paramagnetism
3. Ferromagnetism
4. Ferrimagnetism
5. Antiferromagnetism

2.6.1 Diamagnetism

Diamagnetism is a form of magnetism that is only exhibited by a substance when an external magnetic field is applied to it leading to induced very weak magnetic moment in a direction opposite to the applied field, however in superconductor stronger effect is induced [40] .

Diamagnetism occurs as a result of the non-cooperative behavior of orbiting electrons as it exposed to an applied magnetic field. Thus diamagnetic effect occurs in a

material where magnetic field is due to electronic motion where by the orbiting and spinning completely cancels each other [41].

2.6.2 Paramagnetism

Paramagnetism is a form of magnetism that results from an atom or ions that have permanent magnetic moment where the moments interact with one another weakly and oriented randomly in the absence of an external magnetic field. Thus paramagnetic substances are those with weak magnetic moment having the same direction with the applied magnetic field.

2.6.3 Ferromagnetism

Ferromagnetism also results from a substance with permanent atomic magnetic moments which tend to align parallel to each other even in a weak external field which becomes magnetized after the removal of the external field [41]. Thus ferromagnetic substances are those which create strong magnetization due to the interaction between the magnetic moments of the atoms that cause the alignment of the magnetic moment and remain after the removal of the external field [42]. Some of the semiconductors are found to exhibit ferromagnetism such as (ln,Mn)As , (Ga, Mn)As, ZnO, etc [16].

The ferromagnetic materials can be categorized into two groups; soft magnetic material and hard magnetic materials.

2.6.3.1 Hard Magnet

Hard magnet is a form of a permanent magnets that retain their magnetism after being magnetized. They have large hysteresis loop area resulting to have large hysteresis loss, similarly susceptibility and permeability is low while coercivity and retentivity values are large having higher magnetic energy stored.

2.5.6.2 Soft Magnet

Soft magnet is the type of ferromagnetic material that can easily be magnetized at low magnetic field and demagnetized as well. They are materials with small hysteresis loop area resulting to have low hysteresis loss, similarly susceptibility and permeability are high while the coercivity and retentivity values are low.

2.6.4 Antiferromagnetism

Antiferromagnetism is a situation where by a magnetic ions are arranged such that the moment is pointing in different direction so as to cancel one another where by the exchange interaction between ions in this case has opposite sign and alternate spin arrangement is favored.

2.5.5 Ferrimagnetism

Here also the moments are aligned antiparallel but do not cancel one another due to the difference in magnitude of their moment resulting to have an appreciable resultant magnetization. This type is sometime known as Neel ferromagnetism.

When considering nanomaterials there is a magnetism known as superparamagnetism that appear in a small ferromagnetic or ferrimagnetic nanoparticles where the magnetization can randomly flip direction under the effect of temperature.

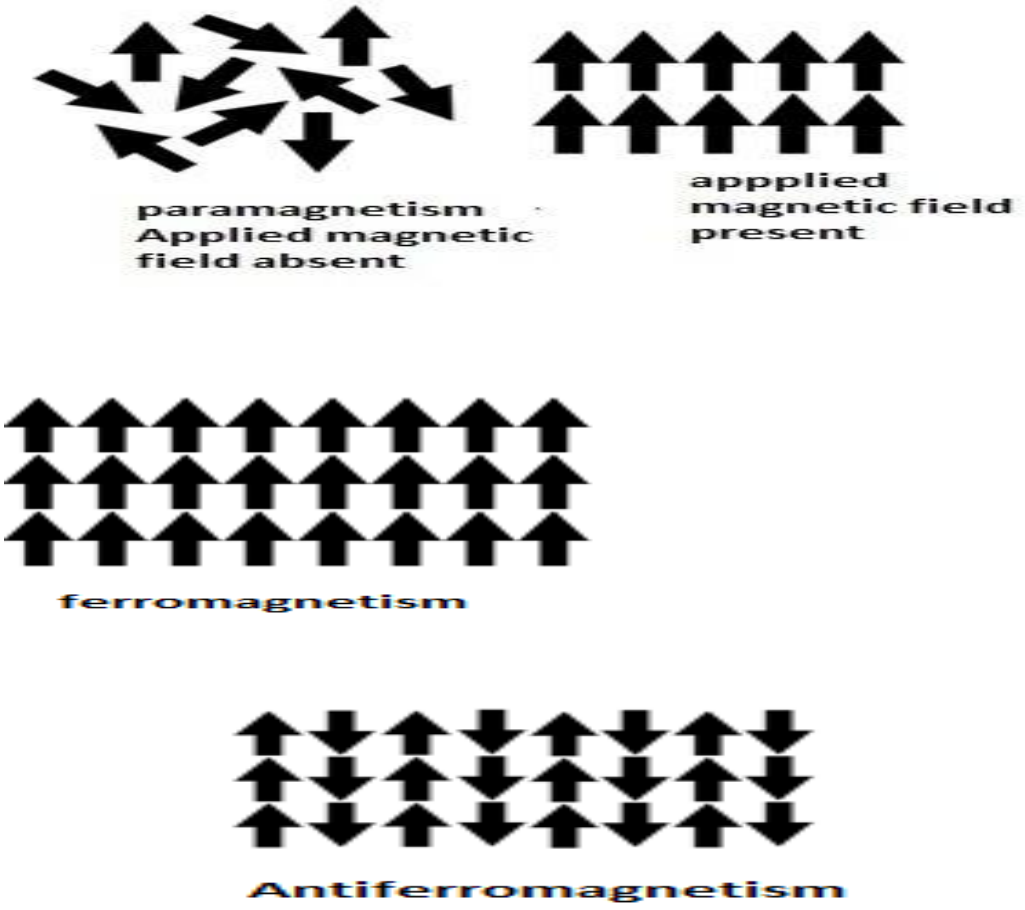

Figure 2.2 Different types of magnetic behaviour.

2.7 CURIE TEMPERATURE

This is a temperature at which certain magnetic materials undergoes a sharp change in their magnetic property or is a temperature at which a Ferromagnetic or Ferrimagnetic material becomes paramagnetic on heating as a result of the alteration of the order of alignment of the ions leading to reduction of the magnetism or even loss the magnetism if heated above the curie temperature. It is also known that dilute magnetic semiconductors have high curie temperature above 300K [1,20,43].

2.8 MAGNETIC DOMAIN

A region where by magnetic fields of atoms are grouped together and aligned is called Magnetic domain which is always present in Ferromagnetic materials because of the way the atoms bond to form the material. When a Ferromagnetic material is magnetized [44], the magnetic domains align parallel to each other to produce a large net field strength in the material and the material becomes magnetic while for the un magnetized material the magnetic domains are randomly oriented so that the magnetic field strength in the piece of material is zero.

2.9 MAGNETIC ANISOTROPHY

The magnetic anisotropy is related to directional dependence having energy known as the crystal energy which describes the dependence of the internal energy on the direction of the magnetization.

2.9.1 MAGNETIC HYSTERESIS

Magnetic hysteresis loop is a form of curve that show the relationship between the induced magnetic flux density (B) and the magnetizing force (H), it is sometimes referred to as B-H loop. Using the loop many information can be deducted about the magnetic properties of a materials. Figure 2 shows the illustration of the loop.

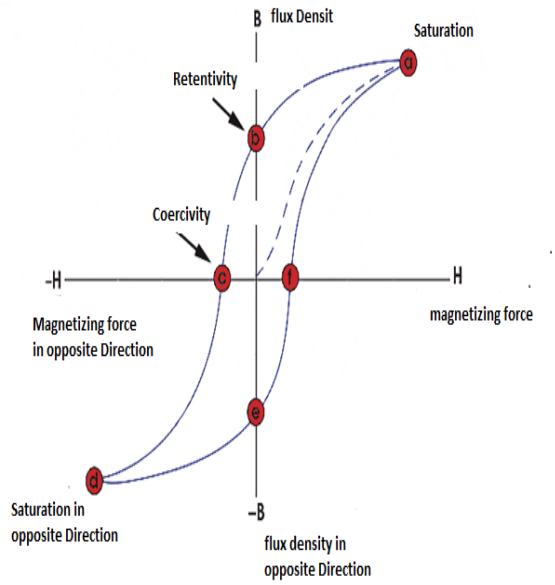

Figure 2.3 Terms in magnetism shown by hysteresis loop [45].

Some terms related to the loop that will help in analyzing magnetic properties of a materials are;

- **Coercivity**: Is a measure of the reverse field needed to derive the magnetization to zero after being saturated. This is to say there is a force which must be applied for a reverse magnetic field of a magnetic material to make the magnetic flux return to zero. (The value of H at point c on the hysteresis curve.)
- **Remanence**: Is a measure of a remaining magnetization when the deriving field is dropped to zero.
- **Retentivity**: Is the ability of the materials to retain some amount of residual magnetic field when the magnetizing force is removed after achieving saturation.
- **Permeability:** Is a property of a material that determines the ease with which a magnetic flux is established in the component .

CHAPTER 3

EXPERIMENTAL STUDIES

Several methods have been employed to achieve the doping process but here we employed microwave synthesis method due to its accelerating rate, versatality of the applied reaction condition, less time consumption, easy to apply and high chemical yield [25].

3.1 SYNTHESIS

To prepare $Mn_xCo_{0.1}Zn_{0.9-x}O$ nanostructured materials with x= 0.00,0.05.0.10,0.15,0.20 molar ratio of Manganase(II) nitrate tetra hydrate ($Mn(NO_3)_2.4H_2O$), Cobalt(II) nitrate hexahydrate ($Co(NO_3)_2.6H_2O$) and Zinc nitrate hexahydrate ($Zn(NO_3)2.6H_2O$) in their respective ratios (see Table 1) were dissolved in 10 mL of doubly distilled water, moreover urea is added as a fuel, and the mixture is stirred with a magnetic stirrer until the mixture dissolved completely. Then the mixture is poured into a curicible which was taken in to a kichen type microwave oven which operates with 800 watts for 15 minutes. The solution boils and dehydrates followed by combustion resulting from the evolution of gas in the form of spark. Then the solution burns completely with the release of much amount of heat and gas, where by obtained the desired solid phase.

Table 3.1 Amounts of Metal Nitrates Used to Synthesize $Mn_xCo_{0.1}Zn_{0.9-x}O$ Nanopowders.

Sample	Mn(II) nitrate (g)	Co(II) nitrate (g)	Zn(II) nitrate (g)	Urea (g)
X=0.00	0.000	0.582	5.346	6.00
X=0.05	0.251	0.582	5.049	6.00
X=0.10	0.502	0.582	4.752	6.00
X=0.15	0.753	0.582	4.455	6.00
X=0.20	1.004	0.582	4.158	6.00

3.2 STRUCTURAL CHARACTERIZATION TECHNIQUES

3.2.1 X-ray diffraction technique (XRD)

This is the method used to identify and characterize a compound based on its diffraction pattern therefore it depends on the duality of a wave-particle to extract information about the structure of a crystalline materials.

X-ray diffraction occurs when an incident beam of monochromatic X–rays interact with a target materials and scattered from atom within the materials. The scattered X-rays in a crystal line structure undergo constructive and destructive interference resulting from diffraction use to identify the crystalline phases present. The Phase identification is accomplished by comparing the positions and intensities of the material's X-ray diffraction peaks against a large library of "standard" diffraction data of known crystalline materials [46].

The above process is described by Braggs law when supposing an incident X-ray beam making an angle θ with one of the crystal plane where by the beam is reflected from both the upper plane and lower planes in which the beam reflected by the lower plane travels farther than the beam reflected by upper plane. So the effective path difference is given by 2dsinθ, the two beams reinforce on some integer multiple of λ which is true for the whole parallel plane as in figure 3.1 which is given as

$$n\lambda = 2d\sin\theta \quad (3.1)$$

The directions of possible diffractions depend on the size and shape of the unit cell of the material. The intensities of the diffracted waves depend on the kind and arrangement of atoms in the crystal structure, the diffractometer used is operating at 40kv and 35mA using Cu Kα as a source. A graphical representation of X-ray beam incident on the lattice is shown in the figure 3.1 below.

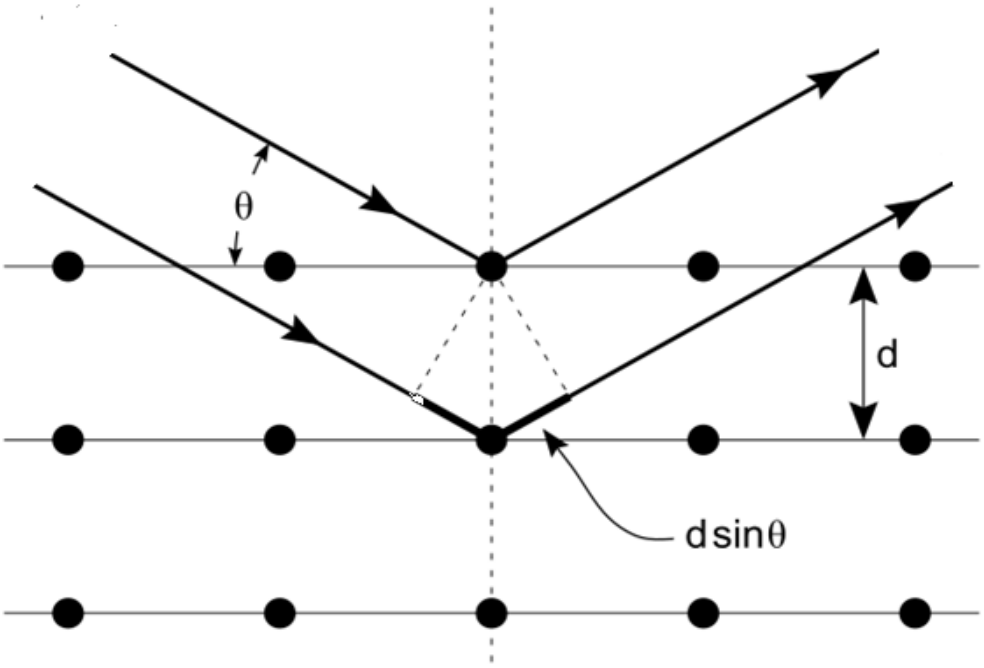

Figure 3.1 X-ray beams incident on a lattice.

To find the sizes of the particles we used Scherer equation which can be written as [13, 15 24]

$$D = \frac{k\lambda}{\beta cos\theta} \tag{3.2}$$

Where, D is the grain size, K is a dimensionless shape factor with a value (0.9) which varies with the actual shape of the crystallite, λ is the wavelength of the x-ray used (1.5402A). B is the full width of the half maximum of the most intense peak, θ is the Bragg angle corresponding to maximum X-ray diffraction peak.

The calculation of the lattice constant a and c can be done by using the formula below for hexagonal system [47].

$$\frac{1}{d^2} = \frac{4}{3}\left(\frac{h^2+hk+k^2}{a^2}\right)+\frac{l^2}{c^2} \tag{3.3}$$

Using Bragg's law we can rewrite the above equation as follows

$$\frac{4sin^2\theta}{\lambda} = \frac{4}{3}\left(\frac{h^2+hk+k^2}{a^2}\right)+\frac{l^2}{c^2} \tag{3.4}$$

where d is the lattice spacing, a and c are lattice constants, hkl are miller indices. To calculate a, we used the peak of the form (hk0) so that c will vanish in the equation, similarly to get c we used the peak that has the form of (002) so that we have only c and l as our variable.

The following equations are derived for a and c respectively.

$$a = \frac{\lambda\sqrt{(h^2+hk+k^2)}}{\sqrt{3}\,sin\theta} \tag{3.5}$$

$$c = \frac{\lambda l}{2sin\theta} \tag{3.6}$$

Figure 3.3.1 picture of X-ray diffraction instrument [Fatih University BİNATAM]

3.2.2 Scanning Electron Microscope (SEM)

A Scanning electron microscope (SEM) is an instrument that is used to produce image of a sample by scanning it with focused beam of high energy electrons used to generate the various signals from the electron beam that interact with the surface of the sample and revealed information about the sample related to morphology, chemical composition, crystalline structure as well as the orientation of the materials making up the sample.

The workability of the instrument is that a beam of electrons is produced at the top of the microscope by an electron gun. The electron beam follows a vertical path through the microscope, which is held within a vacuum. The beam travels through electromagnetic fields and lenses which help in focusing the beam down toward the sample. Once the beam hits the sample, electrons and X-rays are ejected from the

sample which will be detected by backscattered electrons, and secondary electrons which are converted into signal that is sent to a screen where the final image is produced. [47] SEM measurements were done on a high resolution JEOL JSM- 7001F system. A basic representation of SEM is shown in figure 3.32 (a) and (b).

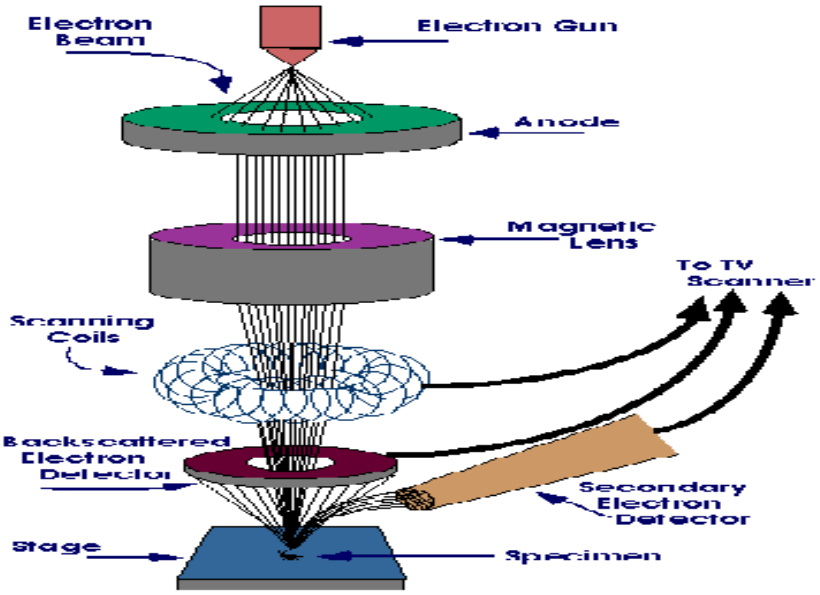

Figure 3.4 Basic representation of SEM.

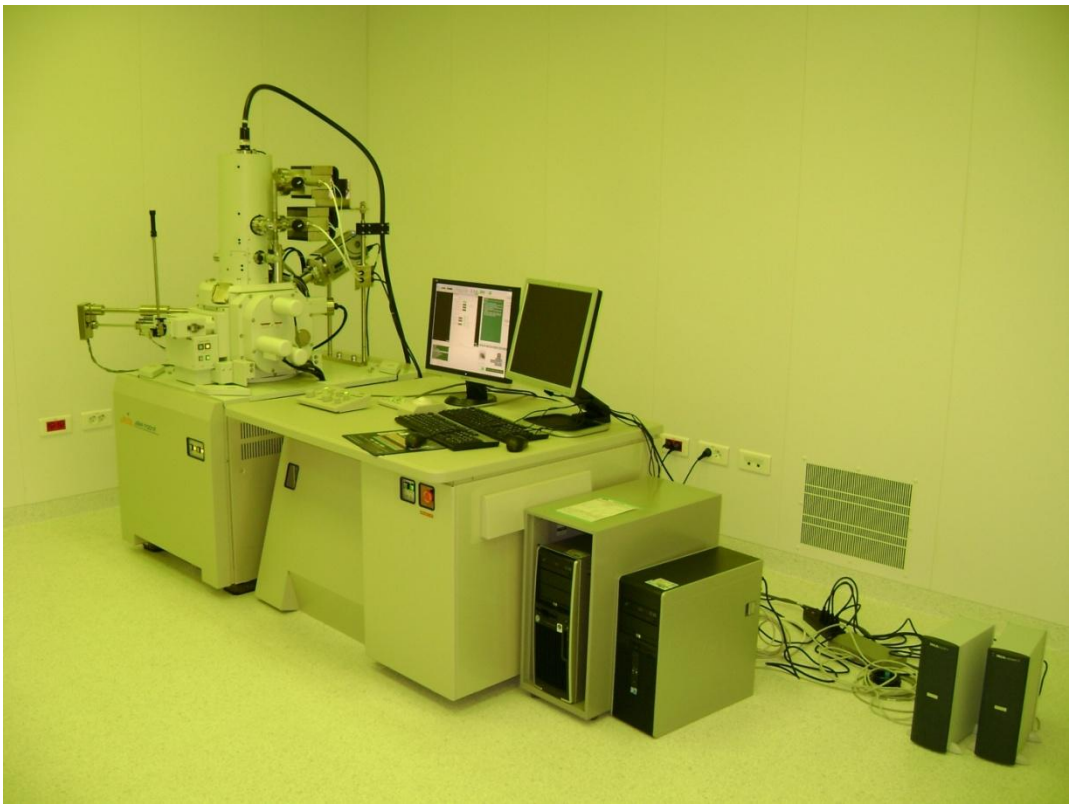

Figure 3.5 Picture of SEM instrument [Fatih University BİNATAM].

3.2.3 Energy Dispersive X-ray Spectroscopy (EDX)

This is another method used for chemical characterization and elemental analysis of the sample. The method results from the interaction of sources of X-ray excitation on the sample. The characterization is under the principle that each element has a unique atomic structure and unique set of peaks on its X-ray spectrum.

The emission of characteristic X-ray from the specimen is been stimulated by a high energy beam of charged particles such as electron or proton, An atom within the sample contain unexcited electron in a discrete energy level bound to the nucleus, the incident beam may excite an electron in the inner shell ejecting it from the shell where by creating electron hole. An electron from outer shell will fill the hole and the different in energy between the higher energy shell and the lower energy may be released in form of an X-ray number and energy of the X-ray emitted can be detected by an energy dispersive spectrometer leading to the detection of the elemental composition of the specimen.

3.2.4 Magnetic Measurements

Magnetic properties of the sample is measured by VSM functionality of quantum design physical property measurement system (PPMS), vibrating sample magnetometers (VSM) is an instrument used to characterize the DC magnetic properties of the sample as a function of magnetic field, temperature and time.

A basic measurement is accomplished by oscillating the sample near a detection pick up coil and synchronously detecting the voltage induced. A sample is vibrated under an external magnetic field produced by an electromagnet which cause change in the magnetic flux density that is detected by the detection coils and transformed to signals which gives details about the magnetization of the sample[48] .

Thus for a relatively large oscillation amplitude (1-3mm) and frequency of 40Hz the system is capable of resolving magnetization changes of less than 10^{-6} emu at a data rate of 1Hz.

Figure 3.34 A picture of quantum design physical property measurement system(PPMS)

3.2.5 Optical Measurements

Many substances absorbed ultraviolet (UV) or Visible light in which the rate of absorption is defined as the logarithmic ratio of the radiation falling upon a material to the radiation transmitted to the material. Similarly the ratio of the incident and leaving electromagnetic radiation through the substances at a specified wavelength is known as **transmittance.**

Meanwhile the amount of electromagnetic radiation (usually light) reflected from a surface to the amount originally striking the surface is called the **reflectance**.

UV-Vis spectrometer is used to measure the optical properties of the sample. It consists of a light source for the spectral range and a tungsten lamp for the visible and IR spectra, having a monochromator for the selection of a single frequency (wave-length) from all those provided by the lamp source to scan over a desired frequency. Moreover a sample holder and a detector used to measure the intensity of each monochromatic beam after traversing the sampled which is finally displayed and the spectra is recorded.

For the powdered crystalline materials diffuse reflectance is an excellent method for analyzing the optical properties of the sample [49,50].

3.2.5.1 Diffuse Reflectance Spectroscopy

When an electromagnetic radiation is directed on to the surface of solid powder, two types of reflection occurs: specular reflection and diffuse reflection (DR). The specular reflection is the direct radiation from the powder sample surface according to the Snell's reflection law; angle of incidence is equal to the angle of reflection. The DR is the radiation that penetrates into powder sample and undergoes to the scattering (it follows many reflections, refractions and diffraction at all directions due to nanostructured mass) and wavelength dependent absorption within the nanomaterial. Some part of this radiation ultimately leaves the bulk sample in all directions. A DR accessory is designed to collect the diffused reflection rather than specular component and directs it into a photo detector. Commonly, the accessory has a spherical surface (integrating sphere) or any other suitable geometry that is coated with a white standard reflecting thin film, Fig.1.

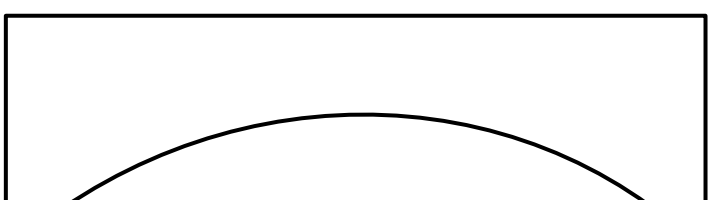

The measurement of DR with a UV-Vis spectrophotometer is a standard manner to determine the optical properties of powder nanomaterials [51, 52]. In the case of semiconducting powder nanomaterials, these properties are potentially the absorption coefficient (*K*) and band-gap energy (or band gap, E_g) [51]. Especially, the *Eg* is an important feature for semiconducting nanopowders which specifies the ability to use for optoelectronic applications. There is no a standard method of powder sample preparation in DR spectroscopy. Usually, powder samples are filled into a rectangular or cylindrical sample holder with a surface of a few ten square millimeters to several square centimeters. The powder nanoparticles should form a 1-3 mm thick layer for all incident light to be absorbed or scattered before reaching the back surface of the sample [52, 53].

The original idea to use the DR spectra recorded from semiconducting nanostructures to calculate the *Eg* was proposed by Kubelka-Munk theory in 1931

[5, 55]. Originally, the theory describes the behavior of light travelling inside a light scattering sample and based on two differential equations:

$$-di = -(S + K)idx + Sjd$$

$$dj = -(S + K)jdx + Sidx \quad (3.6)$$

Here *i* and *j* are the intensities of light travelling inside the sample towards its un illuminated and illuminated surfaces, respectively; dx is the differential part along the light path; *S* and *K* are the scattering and absorption coefficients, respectively. The Kubelka-Munk theory holds for a particle size that is comparable or smaller than the wavelength of incident light and DR no longer permits the secondary contributions of reflection, refraction, and diffraction.

When the thickness of sample is in the relevant limitation then it has no influence on the reflectance. Hence, the Kubelka-Munk equation at any wavelength can be written as

$$\frac{K}{S} = \frac{(1-R_\infty)^2}{2R_\infty} \equiv F(R_\infty) \quad (3.7)$$

where R_∞ is the absolute reflectance and $F(R_\infty)$ is the called as Kubelka-Munk function. In the parabolic band structure, the *Eg* and absorption coefficient are related through the well known Tauc relation [56,57]. The Tauc relation for a direct band gap material is given by the expression

$$\alpha h\upsilon = A\,(h\upsilon - Eg)^n \quad (3.8)$$

where α is linear absorption coefficient, υ is light frequency, and *A* is the proportionality constant. The power of the parenthesis, *n* is taken equal to the 1/2 for direct band gap semiconducting materials. When incident radiation scatters in a perfectly diffuse manner, the absorption coefficient *K* gets equal to 2 α. In this case, considering the scattering coefficient *S* as constant with respect to wavelength, and applying the eq.2 we obtain the relation:

$$[F(R_\infty)h\upsilon]^2 = A(h\upsilon - Eg) \quad (3.9)$$

The $(\alpha h\upsilon)^2$ vs. hυ graph is plotted and the energy-band gap of the powder sample is extracted easily

Figure 3.7 High performance Reliable UV-Vis spectrometer Evolution 300.

CHAPTER 4

RESULTS AND DISCUSSION

4.1 X-RAY POWDER DIFFRACTION (XRD)

Structural characterization of the samples was carried out by using Rigaku X ray diffraction (XRD) spectrometer and Figure 4.1 shows the combined XRD patterns taken from all the samples.

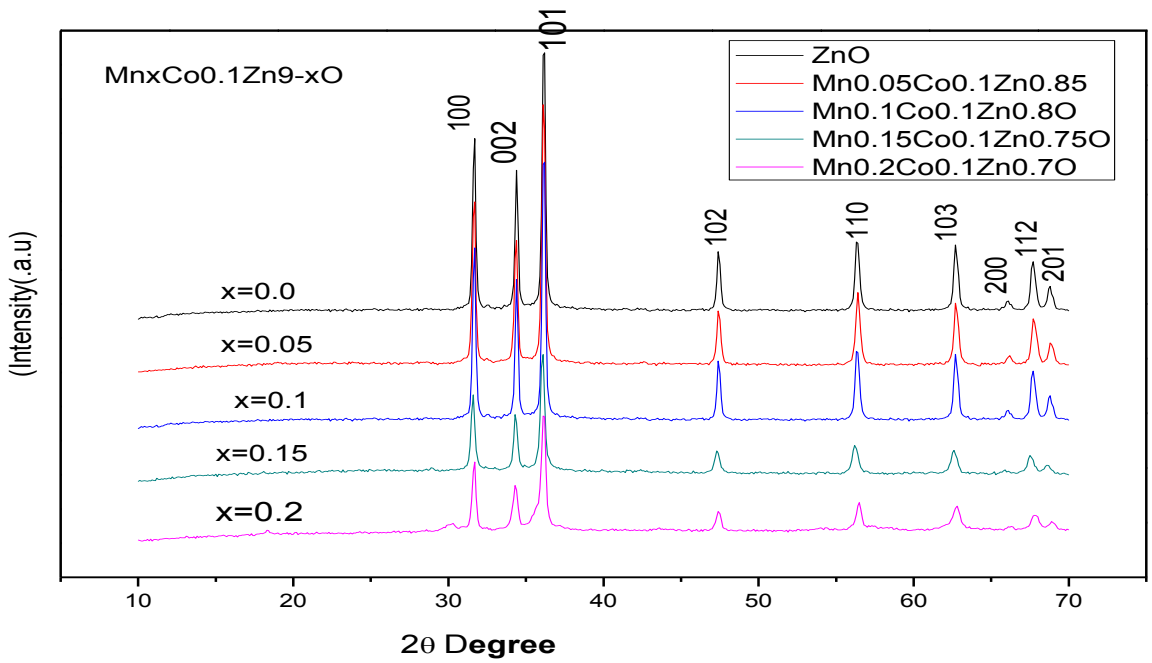

Figure 4.1 XRD patterns for $Mn_xCo_{0.1}Zn_{0.9-x}O$.

We can observe from the XRD patterns that the diffraction patterns indicate the single phase wurtzite structure of ZnO where all the diffraction peaks can be pointed out to the hexagonal phase ZnO as reported in JCPDS card (No. 36-1451, a = 0.3249 nm, c = 0.5206 nm) with nine prominent peaks in which the strong diffraction peaks appear in (100), (002) and (101), respectively [7,43,58]. There are no traces or any other characteristic peaks from Co^{2+} and Mn^{2+} were observed in the samples, therefore it is believed that Co^{2+} and Mn^{2+} can subtitude Zn^{2+} without changing the structure [59,60].

The crystallite sizes of all samples were calculated with Scherrer's equation using the most intense peak (101), where the crystal size lies between 32.65-23.69 as shown in Table 4.11. In addition, the lattice parameters a and c are calculated using (110) and (002) peaks with the help of the classical formula in equation (5 and 6) as presented in the previous chapter.

$$a = \frac{\lambda\sqrt{(h^2+hk+k^2)}}{\sqrt{3}\,sin\theta} \tag{4.1}$$

$$c = \frac{\lambda l}{2sin\theta} \tag{4.2}$$

Table 4.1 Crystal sizes and lattice parameters for all samples.

Sample	D(101) nm	a(110) A	c(002) A
ZnO	32.65	3.2614	5.2085
$Mn_{0.05}Co_{0.1}Zn_{0.85}O$	31.29	3.2610	5.2084
$Mn_{0.1}Co_{0.1}Zn_{0.8}O$	31.18	3.2614	5.2115
$Mn_{0.15}Co_{0.1}Zn_{0.75}O$	25.71	3.2631	5.2143
$Mn_{0.2}Co_{0.1}Zn_{0.7}O$	23..69	3.2636	5.2144

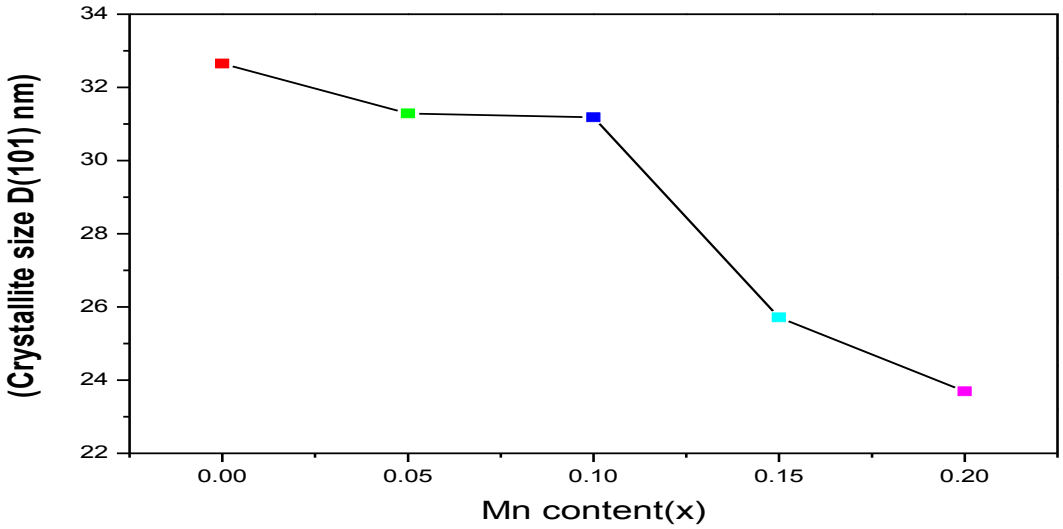

Figure 4.2 Variation of crystalline size of the samples with Mn content.

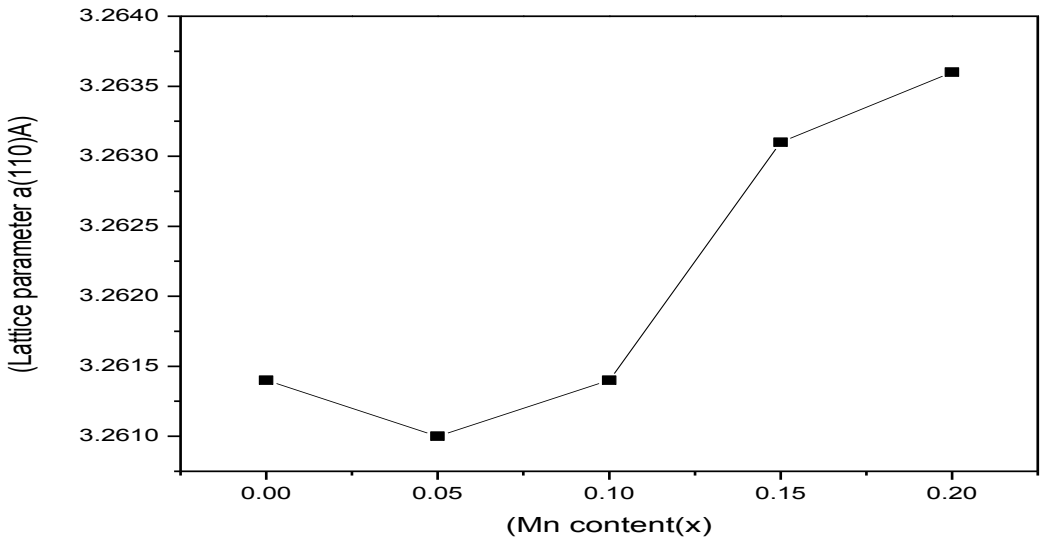

Figure 4.3 Variation of the lattice parameter a for the samples with Mn content.

It can be seen from the Table 4..1 above that the crystallit size of ZnO decreases from 32.65 to 23.69 nm as Mn content increases. Figure 4.2 indicates that addition of Mn^{2+} suppress the growth of ZnO crystal grains.

However there is an increment in the lattice parameters as seen in Figure 4.3 with an increase in Mn^{2+} content which results from the difference in the ionic radii of Co^{2+}, Zn^{2+} and Mn^{2+} with 72, 74 and 80Å respectively.

The theory have shown that the ionic radii of the Co^{2+} is comparable to that of Zn^{2+} while that of Mn^{2+} has a bigger radii compared to $Zn^{2+,}$ thus account for the increment in the lattice parameter of the samples [21,43].However the decrease in the crystal sizes is due to the fact that the intensity of the (101) diffraction peak decreased gradually and the width broadened, which might be due to the increase in the lattice disorder and strain induced by Mn^{2+} substitution.

4.2 SCANNING ELECTRON MICROSCOPE (SEM)

Morphological analysis of the samples was done by using high resolution field effect scanning electron microscopes (FE-SEM JEOL-7001). The FE-SEM images of all samples are shown in Figure 4.4

SEM images reveal that the samples consist of almost spherical shaped nanoparticles and no any indication of phase separation and agglomeration. A close view of particles also shows that smaller crystallites have sizes smaller than 100 nm. Moreover, the nanoparticles were dense and distributed evenly on the whole area. Similarly, these smaller crystallites are so closely arranged together, however, a distinct boundary between neighboring crystallites can still be observed.

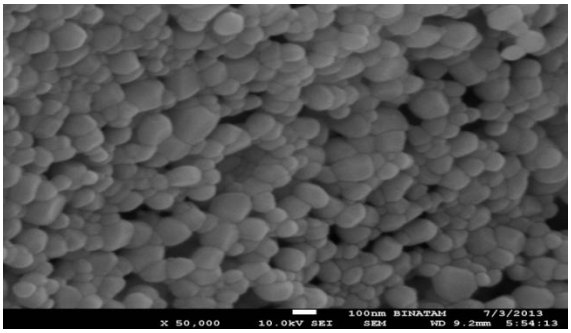

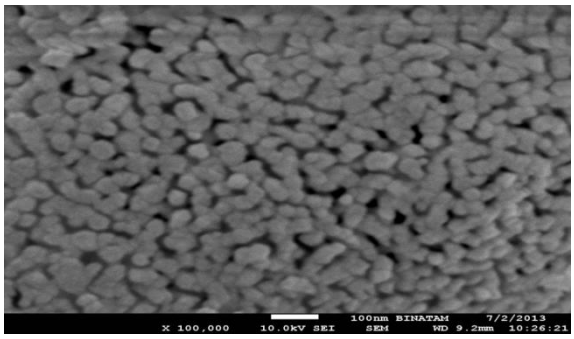

x=0.0

x=0.05

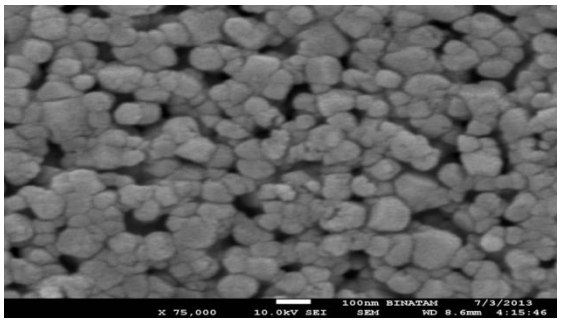

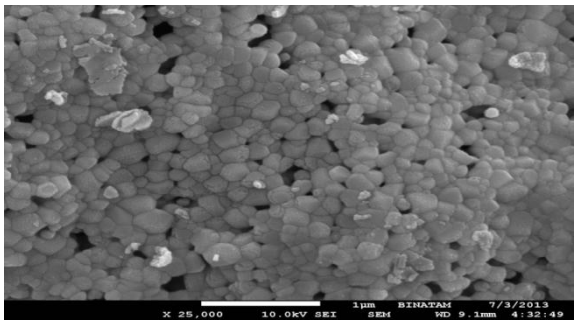

x=0.1

X = 0.15

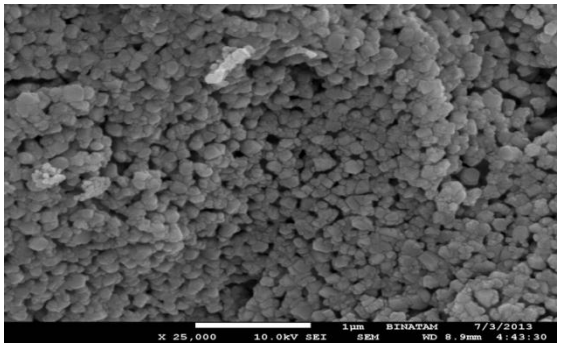

X=0.2

Figure 4.4 Field emission scanning electron micro-graphs (FE-SEM) of $Mn_xCo_{0.1}Zn_{0.9-x}O$ NPs.

4.3 ENERGY-DISPERSIVE X-RAY SPECTROSCOPY MEASUREMENT (EDX)

The elemental compositions of the samples have been studied by Energy-dispersive X-ray spectroscopy **(**EDX). The measurement results comply with what is

expected from the synthesis where by the mass ratios of chemical composition tallies with the outcomes of the EDX spectra. The spectrum contains all the expected elements and no impurity was found.

4.3.1 ZnO Nanoparticles

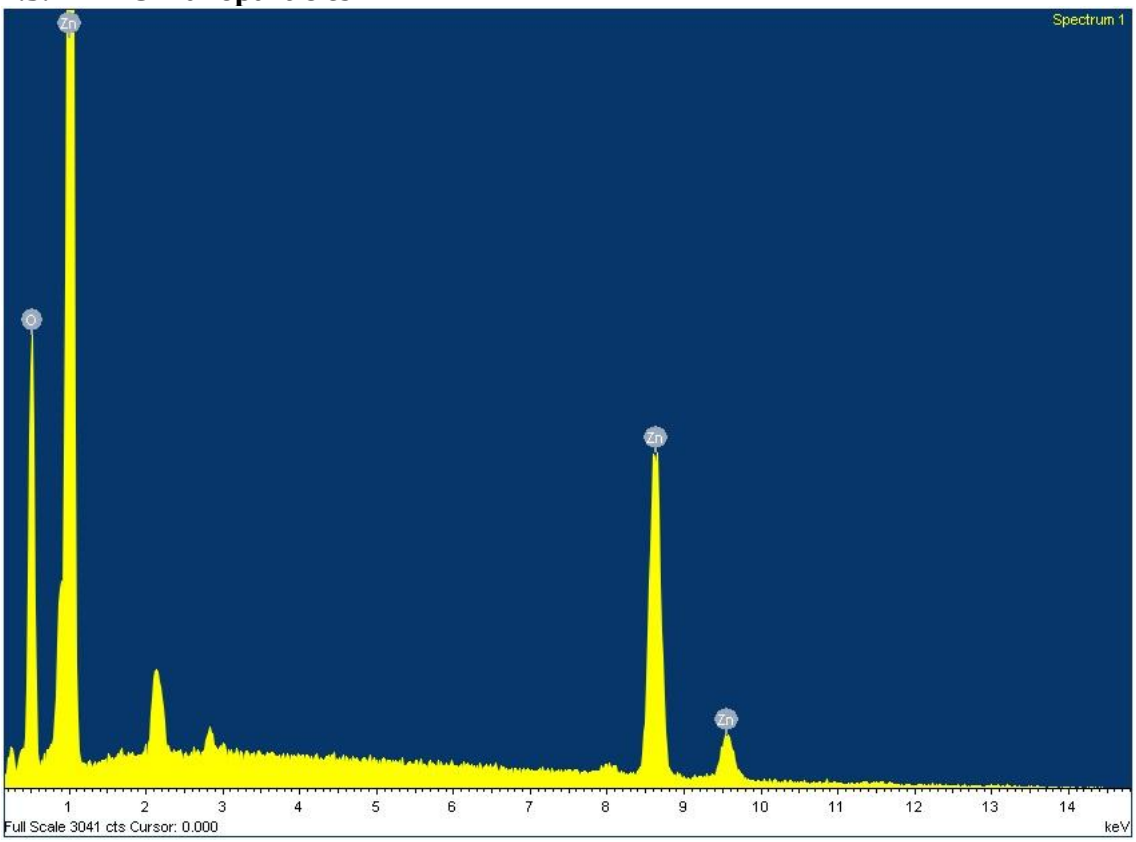

Figure 4.5 EDX graph of ZnO nanoparticles

Figure 4.5 shows the elemental composition of ZnO nanoparticles. From the figure we can observe that the most abundant element is zinc then oxygen. The order depends on the elemental percentage. By using EDX the number of each element in the molecular formula can be deduced from its percent weight.

Table 4.3 Elemental Percentage for ZnO Nanoparticles.

Element	App.conc.	**Inten.Corrn.**	**Weight %**	**Weight % Sigma**	**Atomic%**
OK	8.15	**1.2372**	**6.59**	**0.12**	**56.24**
ZnL	15.82	**0.7556**	**20.94**	**05.1**	**43.76**
Total			**27.53**		

Considering Table 4.3 one can observe that the percentage weight is related with the number of elements in the sample such that the ratio of Zinc and Oxygen is 1:1. However the percentage weight for oxygen is less than the expected value. This indicates that there are oxygen vacancies and oxygen deficiency in the sample's structure. From EDS results the unnamed peaks are due to carbon because before EDS measurements the sample is coated with carbon to produce conductivity.

4.4 $Mn_{0.05}Co_{0.1}Zn_{0.85}O$ NANOPARTICLE

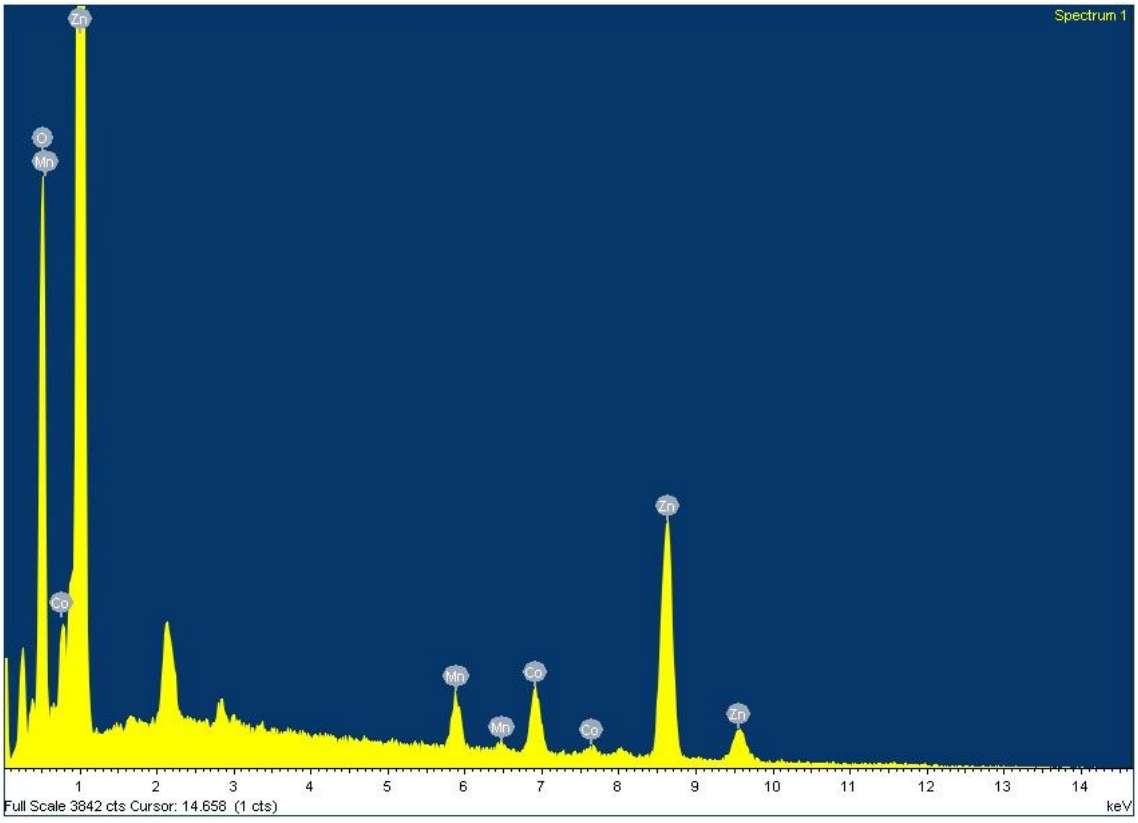

Figure 4.4 EDX graph of $Mn_{0.05}Co_{0.1}Zn_{0.85}O$ nanoparticles.

Fig. 4.4 Shows the elemental composition of $Mn_{0.05}Co_{0.1}Zn_{0.85}O$ nanoparticles. From the figure we can observed that the most abundant element is Zinc then oxygen. The order depends on the elemental percentage. By using EDX the number of each element in the molecular formula can be deduced from its percent weight.

Table 4.4 Elemental Percentage for $Mn_{0.05}Co_{0.1}Zn_{0.85}O$ Nanoparticles.

Element	App.conc.	**Inten.Corrn.**	**Weight %**	**Weight % Sigma**	**Atomic%**

O K	13.67	**1.2726**	**10.74**	**0.15**	**52.68**
Mn K	1.74	**0.9524**	**1.83**	**0.08**	**2.61**
Co K	3.47	**0.9364**	**3.71**	**0.12**	**4.94**
Zn L	20.03	**0.6046**	**33.13**	**0.21**	**39.77**
Totals			**49.41**		

Considering Table 4.4, one can observe that the percentage weights related with the used amount of the chemical materials so as to synthesize the composition of the sample, the number of elements Manganse and Zinc in the sample are in the ratio of 1:17 where by the Percentage weight of manganese shows 1.83 and for Zinc is 33.13. Thus it confirms that the elemental composition match with the experimental results similarly for cobalt. However the percentage weight for oxygen is less than the expected value. This indicates that there are oxygen vacancies and oxygen deficiency in the sample's structure. From EDX results the unnamed peaks are carbon because before EDX measurements the sample is coated with carbon to produce conductivity.

4.5 $Mn_{0.2}Co_{0.1}Zn_{0.7}O$ NANOPARTICLE

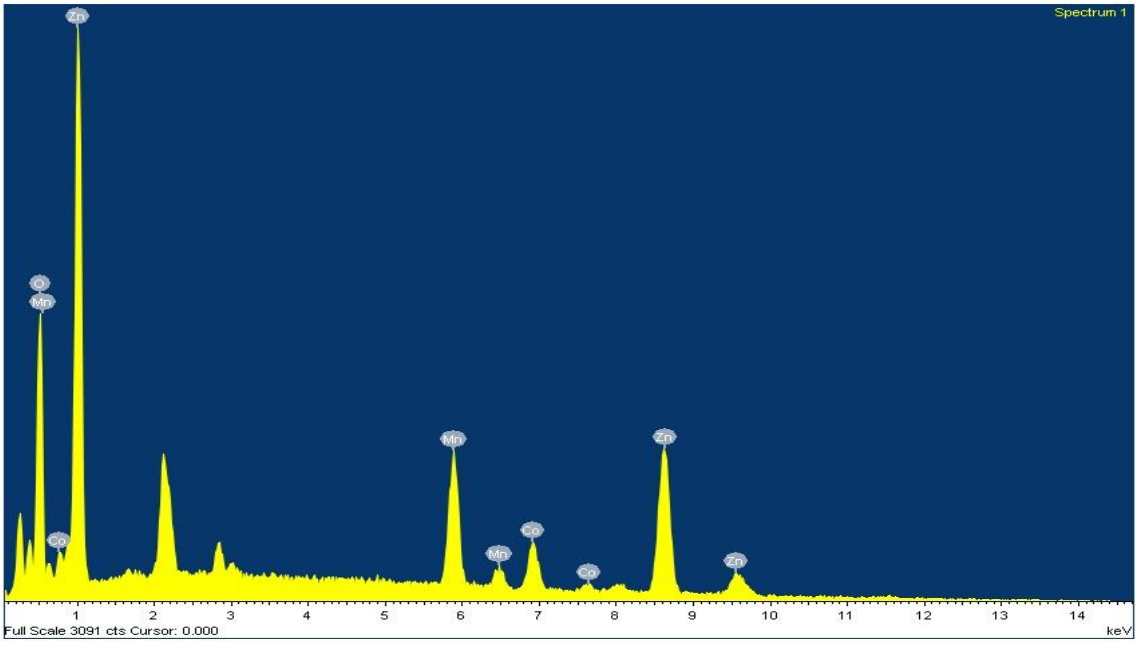

Figure 4.5 EDX graph of $Mn_{0.2}Co_{0.1}Zn_{0.7}O$ nanoparticles.

Figure 4.5 shows the elemental composition of $Mn_{0.2}Co_{0.1}Zn_{0.7}O$ nanoparticles. From the figure we can observe that the most abundant element is Zinc then oxygen. The order depends on the elemental percentage. By using EDX the number of each element in the molecular formula can be deduced from its percent weight.

Table 4.5 Elemental Percentage for $Mn_{0.2}Co_{0.1}Zn_{0.7}O$ Nanoparticles

Element	App.conc.	**Inten.Corrn.**	**Weight %**	**Weight % Sigma**	**Atomic%**
O K	6.83	**1.3823**	**4.94**	**0.1**	**48.77**
Mn K	4.69	**0.9603**	**4.29**	**0.10**	**14.05**
Co K	2.57	**0.9211**	**2.79**	**0.11**	**7.46**
Zn L	5.46	**0.4432**	**12.31**	**0.16**	**29.72**
totals			**24.93**		

With regard to Table 4.5, one can observe that the percentage weight is related with the number of elements in the sample such as the weight of Zinc is almost three half that of manganese. Percentage weight of zinc is 12.31 while that of manganese is 4.29. Therefore the table confirms that the elemental composition match with experimental results. Also the percentage weight for oxygen is less than the expected value. This indicates that there are oxygen vacancies and oxygen deficiency in the sample's structure. From EDX results, carbon is also seen because before EDX measurements the sample is coated with carbon to produce conductivity.

4.4 OPTICAL STUDIES

The Diffuse reflectance spectra (DR) recorded from Mn and Co coordinated zinc oxide powder samples in the (300-1100) nm wavelength region are given in the Fig. 4.4. Since the Co ratio is constant (0.1 at. %) the percent reflectance decreases with increasing Mn concentration.

The pure ZnO samples have an absorption band edge at 372 nm indicating a direct band gap of 3.33 eV which comparable with the room temperature value of 3.37 eV [61,62]. However this band edge is not so sharp like detected ones from many ZnO specimens in the literature [63-66]. In the case of metal doped nanopowders, there are three more absorption bands observed at 566 (2.19 eV), 613 (2.02 eV), and 656 nm (1.89 eV). These three absorption bands are due to interatomic d-d transitions in

tetrahedrally coordinated Co^{2+} ions [67]. The 3-d levels in the Co^{2+} ions undergo splitting due to tetrahedral crystal field formed by O ions. These transitions denoted as (1),(2), and (3) in the Fig.4.4 correspond to

$^4A_2$ (F)→ $^2A_1$(G), $^4A_2$ (F)→ $^4T_1$ (P), and $^4A_2$ (F)→ ^2E(G), respectively, in high spin Co^{2+} [68]. Although, all metal doped ZnO nanoparticles have the same magnitude of Co content, the intensity of these peaks are seem to be comparable just for $Mn_{0.05}Co_{0.10}Zn_{85}O$ and $Mn_{0.10}Co_{0.10}Zn_{80}O$ samples.

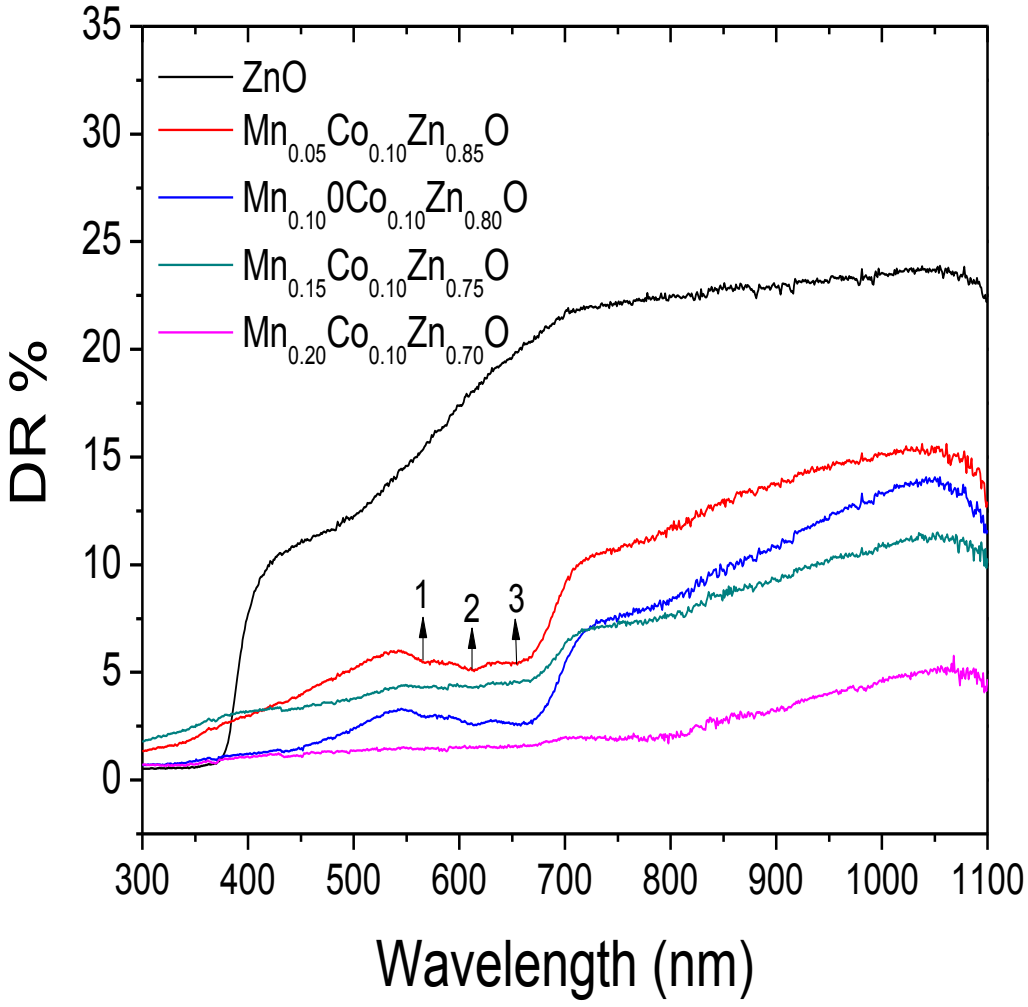

Figure 4.6 (Color online) DR spectra of $Mn_xCo_{0.10}Zn_{1-x}O$ powder samples.

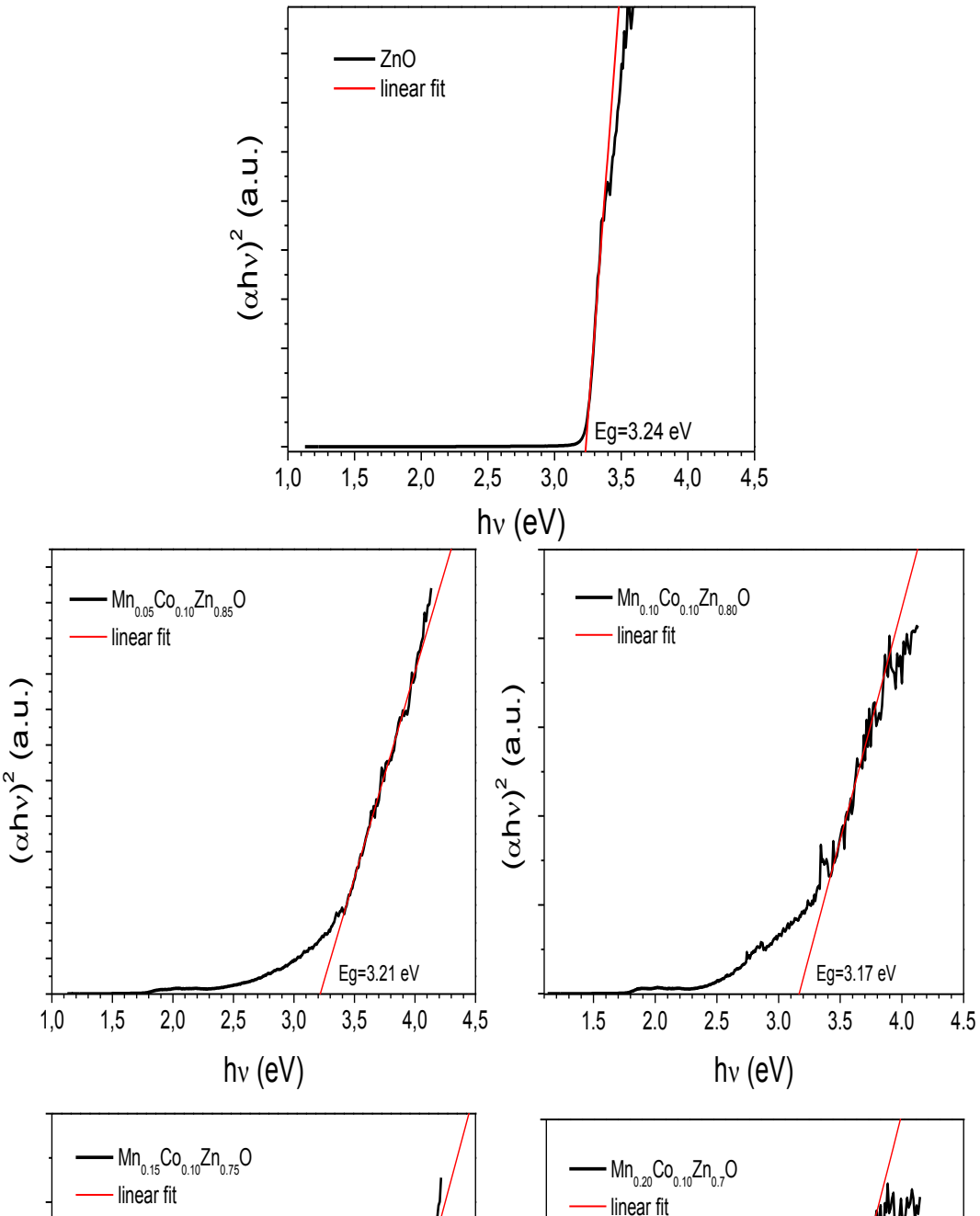
ZnO
linear fit
Eg=3.24 eV
(αhν)² (a.u.)
hν (eV)
Mn0.05Co0.10Zn0.85O
linear fit
Eg=3.21 eV
(αhν)² (a.u.)
hν (eV)
Mn0.10Co0.10Zn0.80O
linear fit
Eg=3.17 eV
(αhν)² (a.u.)
hν (eV)
Mn0.15Co0.10Zn0.75O
linear fit
Mn0.20Co0.10Zn0.7O
linear fit

The *Eg* of the samples were calculated from the Tauc relation given in section three. as eq. 3. The $(\alpha E)^2$ vs E graphs were plotted. In the graphs, a straight line is fitted for the straight segment. The extrapolation of this straight line to the axis of abscissa (*E* axis) gives the band gap values. The Tauc plots of ZnO and $Mn_xCo_{0.10}Zn_{1-x}O$ powder samples and extrapolated E_g values are shown in the Fig.4.42. The samples have decreasing magnitude of 3.24, 3.21, 3.17, 3.16, and 3.02 eV band gap values with respect to Mn content of x=0, 0.05, 0.10, 0.15, 0.20 at. %, respectively. The decrease in the band gap is expected due to increase of carrier concentration.

4.4 MAGNETIC MEASUREMENTS

Magnetic Measurements is characterized by quantum design vibrating sample magnetometer (QD-VSM). The samples were cooled either in the presence of an external magnetic field (field cooling case-FC) or in zero field (zero field cooling case-ZFC), and the magnetic behavior were recorded by sweeping the external field between ±10kOe at different temperatures.

4.4.1 $Mn_xCo_{0.1}Zn_{0.9-x}O$ Nanoparticle

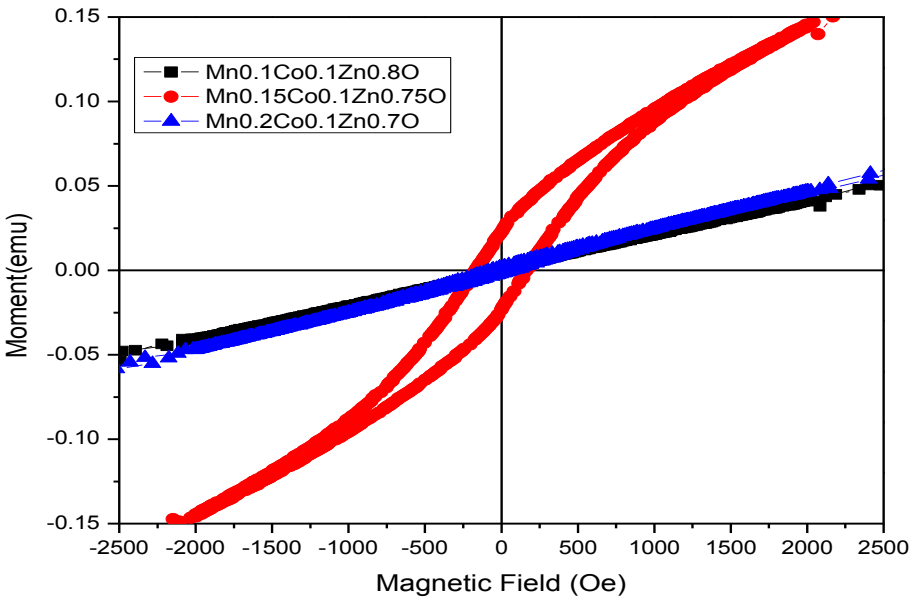

Figure 4.8 The Field-Dependent Magnetization (*M–H* curve) of $Mn_xCo_{0.1}Zn_{0.9-x}O$ Nanoparticles at Room Temperature (*RT*) for all the Samples.

Figure 4.8 shows the field-dependent magnetization (*M–H* curve) of $Mn_xC_{o0.1}Zn_{0.9-x}O$ nanoparticles at room temperature (*RT*). The measurement, reveal that the samples show paramagnetic and Ferromagnetic behavior. The paramagnetic behavior can be attributed to the incorporation of Mn ions in ZnO structure[7,43,60], however for all Mn Concentration there is no linear variation of magnetic moment with Concentration of Mn whereby at x=0.15 the samples show Ferromagnetic behavior even at room temperature with formation of S Shape magnetic hysteretic loop having a saturation magnetization (Ms) with the indication of and coercive field (Hc) and remanent magnetization M_r of 47.70Oe and $1.8x10^{-1}$ (emu/g), respectively [69,70]

4.4 $Mn_{0.1}Co_{0.1}Zn_{0.8}O$ NANOPARTICLE

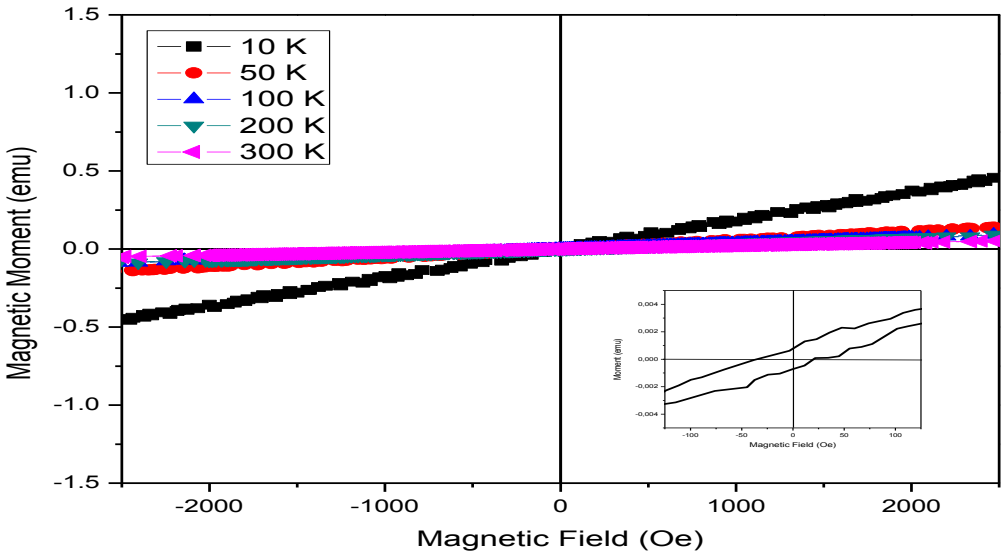

Figure 4.9 The M-H Curves of $Mn_{0.1}Co_{0.1}Zn_{0.8}O$ Taken at Different Temperatures.

As can be observe from Fig4.42 the value of magnetization decrease by increasing temperature showing paramagnetic behavior which may due to the formation and growth of grains. The increase in temperature increase the thermal agitation of the atoms which result in the non alignment of the atoms in the magnetic field hence the magnetization of the material decreases .however there is still ferromagnetic contribution at low magnetic field.

Therefore the sample obeys curie's law which stated that the increase in the strength of the applied magnetic field leads to an increase in the magnetization of the paramagnetic magnetic materials as shown in the figure4.42 thus magnetization varies inversely with temperature as given by the equation

$$\frac{M}{H} = \frac{Co}{T - \theta o} \qquad (4.3)$$

where C is the Curie constant, T is the temperature in Kelvin and B is the applied magnetic field.

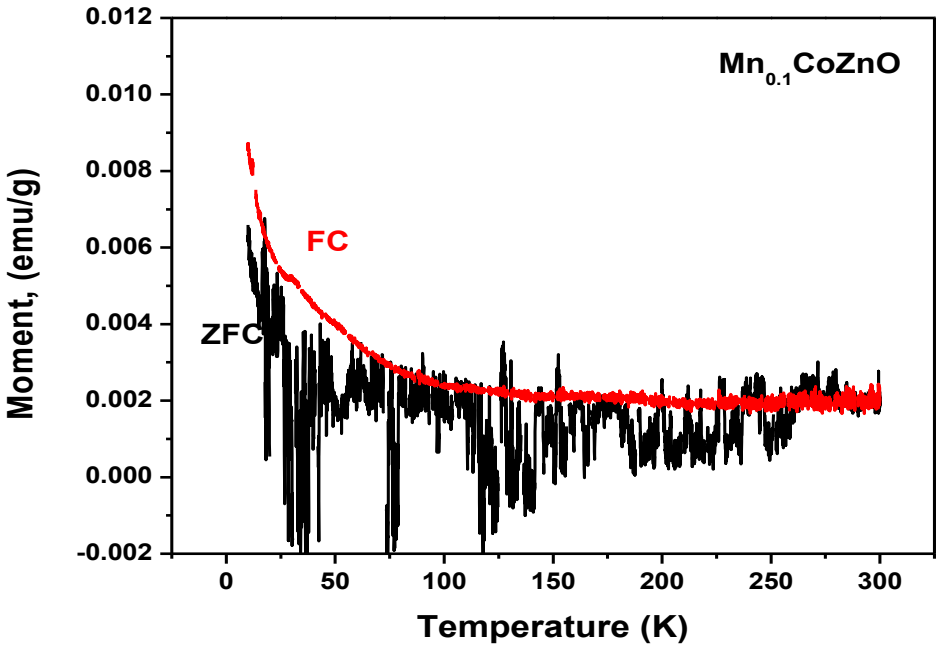

Figure 4.10 M-T Curve for $Mn_{0.1}Co_{0.1}Zn_{0.8}O$ in Zero Field Cooling (ZFC) and Field Cooling(FC).

Figure 4.10 shows the temperature dependent magnetization curves, during zero field cooling (ZFC) and field cooling (FC) in an applied magnetic field of 500Oe, From the figure we can observed that the sample show little ferromagnetic behavior in the temperature range of 10-300k. The magnetization decrease as the temperature increase which behave strictly as paramagnetic behavior [25,59,71,]

4.4.3 $Mn_{0.15}Co_{0.1}Zn_{0.75}O$ Nanoparticle

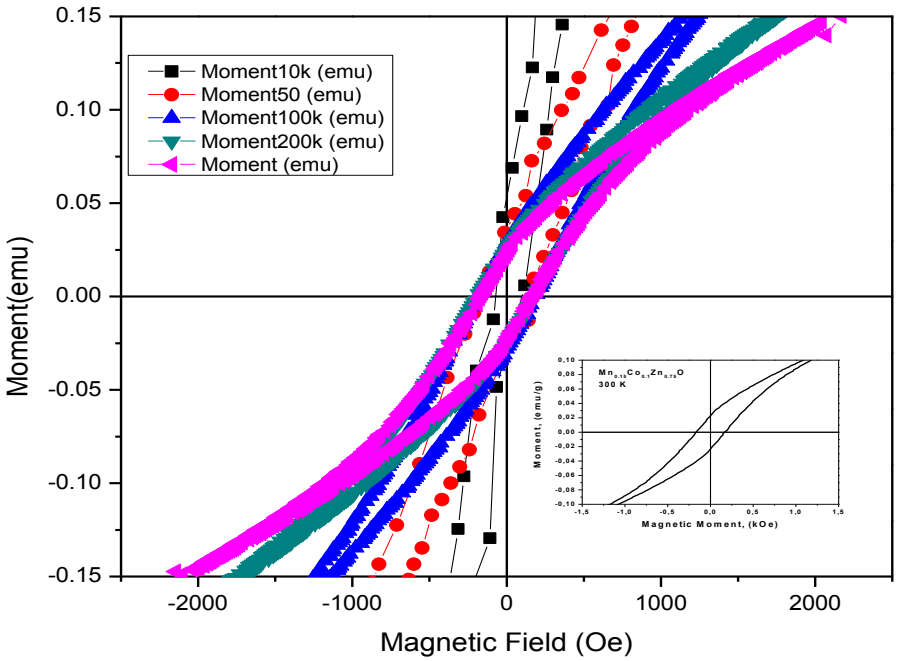

Figure 4.11 The M-H Curves of $Mn_{0.15}Co_{0.1}Zn_{0.75}O$ Taken at Different Temperatures.

As can be seen from Figure 4.43a, the graph of $Mn_{0.15}Co_{0.1}Zn_{0.75}O$ at all temperature, It can observed from the figure that the low-field magnetic hysteretic loop (0–1000 Oe) shows ferromagnetic behavior, with coercive field H_c= 47.70Oe and remanent magnetization M_r= $1.8x10^{-1}$ (emu/g), where as high-field (above 1,000 Oe) hysteresis indicates paramagnetic property.

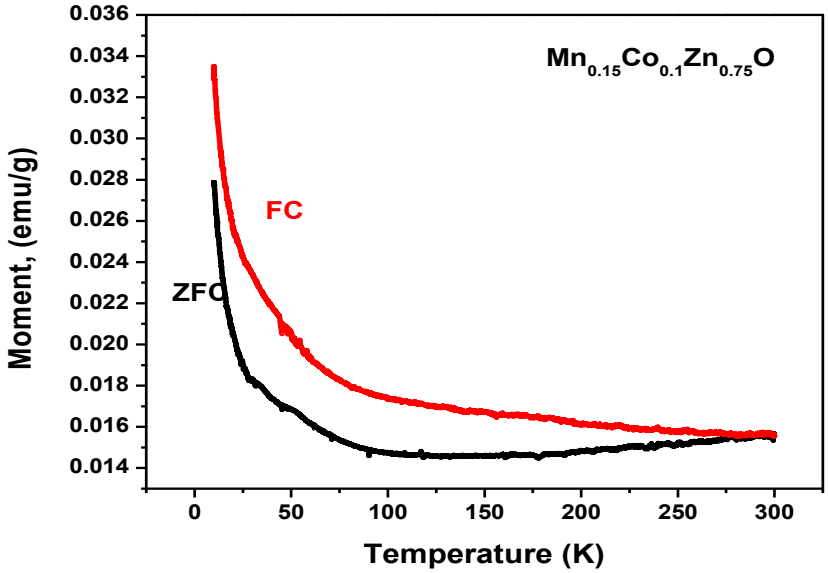

Figure 4.12 M-T curve for $Mn_{0.15}Co_{0.1}Zn_{0.75}O$ in Zero Field Cooling (ZFC) and Field Cooling (FC)

Figure 4.12 shows the temperature dependent magnetization curves, during zero field cooling (ZFC) and field cooling (FC) in an applied magnetic field of 500Oe, From the figure we can observed that the sample diverge at a temperature 295k which show ferromagnetic behavior at room temperature. [25,71,72.]

4.4.4 $Mn_{0.2}Co_{0.1}Zn_{0.7}O$ Nanoparticle

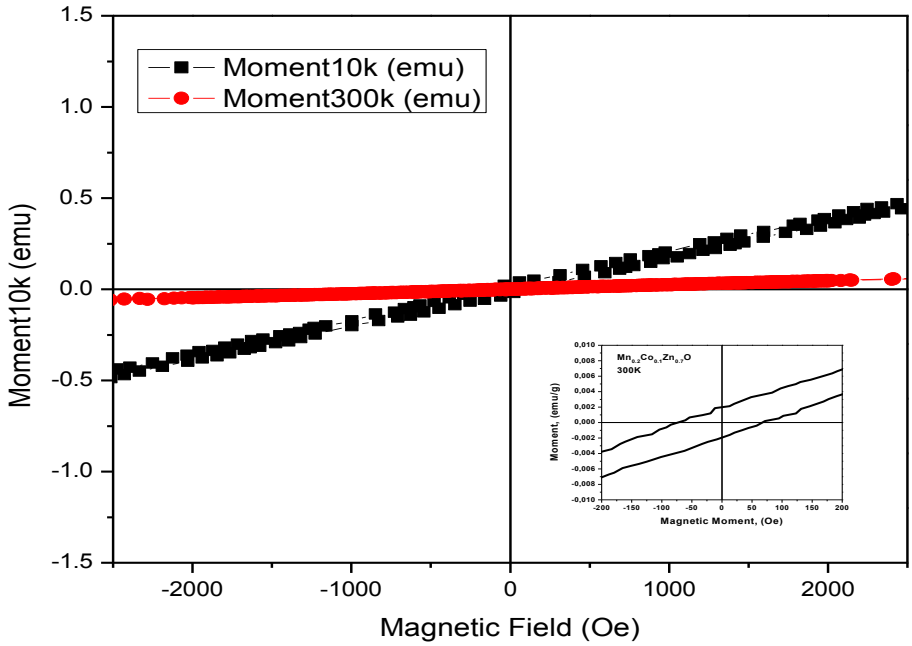

Figure 4.13 The M-H Curves of $Mn_{0.2}Co_{0.1}Zn_{0.7}O$ Taken at Different Temperatures.

As can be seen from Figure 4.13 the value of magnetization decrease by increasing temperature, Moreover the graph of $Mn_{0.2}Co_{0.1}Zn_{0.7}O$ at all the temperature shows paramagnetic behavior which may due to the formation and growth of grains. The slope of the curve M–H (dM/dH) decreases with temperature [43] where by Curie's law is obeyed as shown in Figure 4.9.4 .however there is still ferromagnetic contribution at low magnetic field.

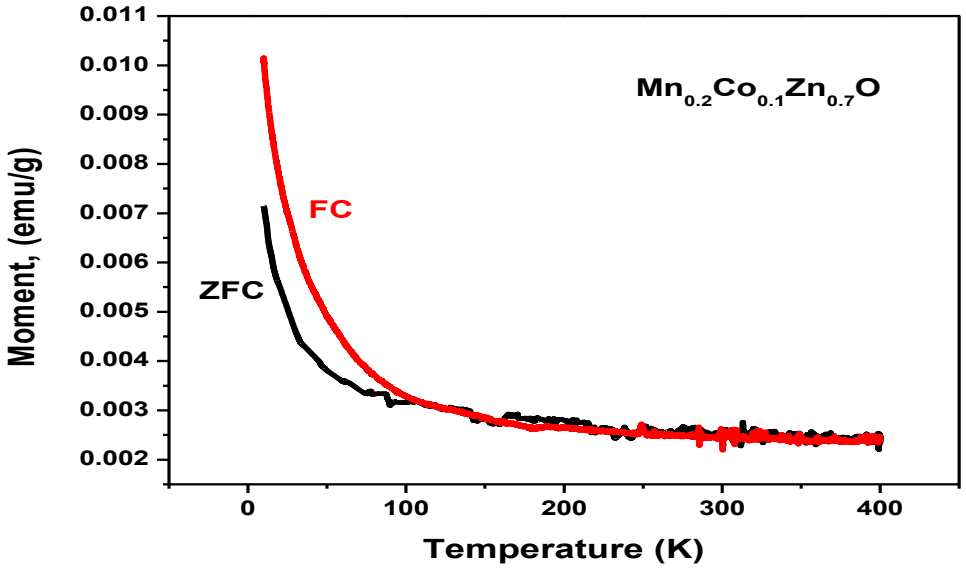

Figure 4.14 M-T Curve for $Mn_{0.2}Co_{0.1}Zn_{0.7}O$ in Zero Field Cooling (ZFC) and Field Cooling (FC)

Figure 4.14 shows the temperature dependent magnetization curves, during zero field cooling (ZFC) and field cooling (FC) in an applied magnetic field of 500Oe, From the figure we can observed that the magnetization decrease as the temperature increase and a rapid increment occur at lower temperature which indicate a paramagnetic behavior however the sample diverge at a temperature 105k where the difference in the FC and ZFC is a sign that indicate ferromagnetic contribution exhibited by the sample at low temperature. [25,71.

CHAPTER 5

CONCLUSION

$Mn_xCo_{0.1}Zn_{0.9-x}O$ nanoparticles with x= 0.0, 0.05 0.1, 0.15, and 0.2 has been successfully synthesized by microwave assisted combustion synthesis method using urea as a fuel. Its structural, morphological, compositional, magnetic as well as optical properties were investigated using X-ray diffraction (XRD), Scanning electron microscopes (FE-SEM JEOL-7001), Energy-dispersive X-ray spectroscopy (EDX), Vibrating sample Magnetometry (VSM) in Quantum Design Physical Property Measurement System (PPMS) and UV-Visible spectroscopy, respectively.

The X-ray diffraction pattern (XRD) measurements of the samples showed the formation of single phase wurtzite structure of ZnO without any indication of secondary phases. Moreover the crystallite sizes of all samples were calculated with Scherrer's equation where the average crystallites size lies between 32.65-23.69 nm as a result of the decrease in the intensity of the (101) diffraction peak and increase in the FWHM this indicate that the crystallinity of the sample increase as a result of compactibility of the atoms in the crystals which might be due to the increase in the lattice disorder and strain induced by Mn^{2+} substitution.

In addition the lattice parameters a and c increases with an increase in Mn^{2+} content which results from the difference in the ionic radii of Co^{2+} , Zn^{2+} and Mn^{2+} with 72, 74 and 80Å respectively where by Mn^{2+} has greater radius compared to Zn^{2+} this account for the increament in the lattice parameters of the sample.

Scanning electron microscopes (FE-SEM JEOL-7001) images of all samples reveal that the samples consist of almost spherical shaped nanoparticles and no any indication of phase separation and agglomeration. A close view of particles also shows

that smaller crystallites have sizes smaller than 100 nm. the nanoparticles were dense and distributed evenly on the whole area. Similarly, these smaller crystallites are so closely arranged together, meanwhile a distinct boundary between neighboring crystallites can still be observed.

Moreover, the Energy-dispersive X-ray Spectroscopy (EDX) measurement results comply with what is expected from the synthesis where by the mass ratios of chemical composition tallies with the outcomes of the EDX spectra. The spectrum contains all the expected elements and no impurity was found meanwhile the percentage weight for oxygen is less than the expected value, this indicates that there are oxygen vacancies and oxygen deficiency in the sample's structure. However the presence of carbon in the samples results from the coating before the EDX measurement so as to produce conductivity.

The Magnetizations of the samples were characterized using Vibrating Sample magnetometer (VSM) functionality of Quantum Design Physical Property Measurement System (PPMS). The magnetization measurements of $Mn_xCo_{0.1}Zn_{0.9-x}O$ nanoparticle reveals that the sample shows paramagnetic and Ferromagnetic behavior the paramagnetic behavior can be attributed to the incorporation of Mn ions in ZnO structure however for all Mn Concentration there is no linear variation of magnetic moment with Concentration of Mn whereby at x = 0.15 the samples show Room temperature Ferromagnetic behavior with non zero coercive field and remanent magnetization.

Similarly the temperature dependent magnetization curves, during zero field cooling (ZFC) and field cooling (FC) in an applied magnetic field of 500Oe, Shows the confirmation for the room temperature ferromagnetic behavior in 0.15 sample and possibility of low temperature ferromagnetic contribution presence in 0.2 sample

The Diffuse reflectance (DR) spectra were recorded from Mn and Co Coordinated zinc oxide powder samples in the (300-1100) nm wavelength region. It indicates that the percentage reflectance decreases with increasing Mn concentration.

The energy band gap *Eg* of the samples were calculated from the Tauc relation The samples have decreasing magnitude of 3.24, 3.21, 3.17, 3.16, and 3.02 eV band

gap values with respect to Mn content of x=0, 0.05, 0.10, 0.15, 0.20 at.% respectively. The decrease in the band gap is expected.

REFERENCES

[1] Mohapatra, J., Mishra, D.K., Mishra ,D., Perumal ,A., Medicherla, V.R ‘’Room temperature ferromagnetism in Co doped ZnO within an optimal doping level of 5%’’*Material Research Bulletin,*47 1477-1422, (2012).

[2] Impex, M.K., *Nanotechnology application,* 2009. http//:www.mknano.com.

[3] Feynman, R., *Fundamental concept of Nanotechnology,* 1980. http//:www.nano.gov/nanotech-101/what/defnition.

[4] Yoshhimura,Byrappa K. ‘’ Hydrothermal Processing of Materials, Past, Present and Future’’ *Journal of Material Science,* 43 (2008).

[5] Hao, Y.M., Lou,S.Y., Zhou, S.M., Zhou,R.J., Yuan, G.Y.Z.,and Ning L., ‘’Structural,optical, and magnetic studies of manganese-doped zandinc oxide hierarchical microspheres by self-assembly of Nanoparticles’’ *Nanoscale Research letter.* 7:100, (2012).

[6] Sentos,A., Daniel,A., Mac-edo, M.A., ‘’Study of the magnetic and structural properties of Mn, Fe, and Co-doped ZnO powder’’ *physica B* 4078, 3229-3232 . (2012).

[7] Sharma,V.K., Najim, M., Srivastava A.K., Varma, G.D.’’Structural and Magnetic Studies on Transition Metal (Mn, Co) doped ZnO Nanoparticles’’ *Journal of Magnetism and Magnetic Materials* 324: 683-689, (2012).

[8] Band, M., Meyer, D.,’’Nanotechnology’’*Physics Review B,* 67035403 (2003).

[9] David, A ,*Zinc Oxide (ZnO) Nanoparticles, Properties, Applications,* (2005). http//:www. Azom.com/ads/abmc.com

[10] Ozgür U, Alivov. Y.I., Liv, C. Teke, A.,Reshchikov, M. A., ‘’A comprehensive review of ZnO materials and devices’’ *Journal of Appl. Phy.* 98, 041301 (2005);

[11] Fang, G., Jia L.,’’Zinc Oxide Nanostructures: Synthesis and Properties’’ *University of California, Irvine, CA 92697, USA* 22 April, 2005.

[12] Garcia M.A.,’’Magnetic properties of ZnO nanoparticles'' *Nanoletter Volume7* No.61489-1494(2007)

[13] Köseoğlu, Y.,'' Enhanced Ferromagnetic Properties of Co-doped ZnO DMS Nanoparticles'' *Supercond Nov. Magn* 26:485-489 (2013).

[14] Yang, Z.,''A perspective of recent progress in ZnO diluted magnetic semiconductors'' *Appl. PhyA material science*, 112.241-254 (2013).

[15] Kaushik, A., Dalela, B., Rathore, R., Vats, V.S., Choudhary, B.L., Alvi, P.A., Kumar, S.,Dalela, S.,'' Influence of Co doping on the structural, optical and magnetic properties of ZnO Nanocrystals'' *Journal of Alloy and compound*, 578 328-335(2013).

[16] Reber R. R.''theory of circularly polaarized X-ray'' *Journal Appl. Phy* 41 5068 (1970)

[17] Thomas, D.G., ''Solid tate communications''*Journal Physics,chemistry*, 1586 (1960).

[18] Collins, R. J. and Kleiman, A.,'' optical and physical properties of some IR Spectroscopy *Phy,Chem Solid*, 190 (1959).

[19] Babu, B., Ramakrishna,C.,''Molecular and Biomolecular spectroscopy'' *Spectromica Acta partA* 109 90-96, (2013).

[20] Caglar,Y.,''Sol–gel derived nanostructure undoped and cobalt doped ZnO Structural,optical and electrical studies '' *Journal of Alloy and compound* 560 181-188, (2013).

[21] Sharma, P., Gupta, A.,Rao, K.V.,Owens, F.J.,'' Origion Ferromagnetism in thin film and nanoparticles of inorganic materials'' *Nat.matter* 2 673 (2003).

[22] Jin, Z., Fukumura, T., Kawasaki, M.,'' nanoscale materials from science and technology *Appl. Phys. Letter*, 78, 3824 2001.

[23] Fukumura, T., Jin, Z., Kawasaki, M.**''**Antiferromagnetisminbulk$Zn_{1-x}Co_xO$ magnetic Semiconductors prepared by the coprecipitation techniq'' *Appl. Phy. Letter* 78 958 2001.

[24] Köseoğlu,Y.,'' A simple microwave-assisted combustion synthesis and Structural,optical an magnetic characterization of ZnO nanoplatelets '' *Ceramics International*39 4221-4230, (2013).

[25] Ajwafi,R.N.,Rahman, F., Mujasam, K. B.,''Surface defect mediated magnetic interactions and ferromagnetism in Cr/Co Co-doped ZnO Nanoparticles'' *Journal of Magnetism and Magnetic Materials* 332130-136, (2013).

[26 Tang,G.,Shi,X., Huo, C., Wang, Z., ''Room temperature Ferromagnetism in Hydrothermally grown Ni and Cuco-doped ZnOnanorods'' *Ceramics International* 39 4825-4829, (2013).

[27] Neamen,D.A., *Semicondıctor Physics and devices Second edition* 1997.

[28] Shin, S.W.. *Surface and coating technology* 231 364-369, (2013).

[29] Fu. J.L., Pen X.,Yan. S.,Gong,Y., Tan,Y., Liang, R., Du, R., Xing, X.,'' Synthesis and structural characterization of ZnO doped with Co'' *Journal of alloy and Compound* 558 212-221, (2013).

[30] Farlex, F.R., *Intrinsic semiconductors,* 2013. http://www.thefreedictionary.com/İntrinsic+semicondctor

[31] Tian,X.,Pan,X.,Zhang,Z Fan,H.,Zeng,X.,Xiao,C.,Hua,G., Wei,Z., '' Growth and Characterization of the Al-doped and Al–Sn co-doped ZnO nanostructures'' *Ceramic İnternational* 39 6497-6502, (2013).

[32] Athren ,T., Solid state physics Crystalline Solids (2013). Hyperphysics. Phy-astr.gsu. edu/hbase/solid/dope.html

[33] Tong Y.H., Liu ,T. Y.C., ''The Optical Properties of ZnO Nanoparticles Capped with Polyvinyl Butyral''*Journal of sol-gel science and technology,* 30 157-161 2004.

[34] Abbas, K. N., *Khalid T. Al- Rasoul K. , Shanan,Z .J ''* New Method of Preparation ZnS Nano size at low pH '' *International. Journal of lectrochemical science,* 8 3049-3056, (2013).

[35] Dharmal J.,'' Simple Method of Measuring the Band Gap Energy Value of TiO2 in the Powder Form'' *UV/VIS/NIR Spectrometer Application* 2009-2012.

[36] Kashimbila, M.M., Electricity ,Magnetism and Modern Physics second edition 2009.

[37] Softlayer,I.B.M., *Magnetism* 2012. http://www.infoplease.com/encyclopedia/science/magnetism.html

[38] BU,S.F.,*Magnetic Particles Inspection*. 2013. http://www.org/educationRes/communityCollege/magpart/Phy/magnetism.html

[39] BU, S. F.**,** *Classes of magnetic materials* 2013. http://www.irm.umn.edu/hg2m/hg2m-b.html

[40] SA, C.CY., *Diamagnetism* 2013. http://www.princeton.edu/~achaney/tmve/wiki100k/docs/Diamagnetism.htm

[41] John W. Jewett. Jr. Raymond A. *Serway Physics for scientist and engineers with Modern physics seventh edition* 2008.

[42] Britannnica, E.,Ferromagnetism 2013. http://www.britannica/EBcheked/topic/205135/ferromagnetism.

[43] Siddheswaran R. Mangalaraja, V., Gómez M E., Ricardo E. Avila, C., Esther J. ''Room temperature ferromagnetism in combustion synthesized nanocrystalline Co, Al co-doped ZnO'' *Journal of Alloy andCompound* 581 146-149, (2013).

[44] NDT; R., *Introduction to the Mystery of Magnetism* http://www.ndt.org/educationResources/highschool/magnetism/twoends.html

[45] Tan, M., *Low temperature magnetic and Dielectric propertiesof Cr doped Ni-Zn Nanoferrites,* M.S thesis Fatih University 2013.

[46] XOS, *Micro X-ray diffraction (μXRD)* 2013. http://www.xos.com/techniques/xrd

[47] Purdue,,U.,*Radiologyical and Environmental management* 2013. http://www.purdue.edu/rem/rs/sem.htm

[48] EBR, *VSM options user manual* febuary 2011. http://www.mrl.ucsb.edu/.../VSM%20manual%B0 VSM option user's Manual 1096-100 Rev.

[49] Barton,and David G. . *Journal of Phys. Chem B,* 103 630-640 1999.

[50] Cindy, F., Baulsir, Thomas,J., Tague, J.,'' Introduction to Diffuse Reflectance Infrared Fourier transform spectroscopy'' *technical notes,* 2003.

[51] W. W. Wendlant, H. G. Hecht,'' Reflectance spectroscopy'', *Wiley Interscience, New York,* 1966

[52] A.B. Murphy, ''Solar Energy'' *Materials and Solar Cells* 911326-1337, (2007).

[53] J. Torrent and V. Barron, *Encyclopedia of Surface and Colloid Science, Marcel Dekker Inc.: New York 2*002.

[54] P. Kubelka and F. Z. Munk, *Tech. Phys.* 12 593 (1931).

[55] A. E. Morales, E. S. Mora, and U. Pal, Revista Mexicana De Fisica S 53 (5) 18-22 (2007).

[56] G.P. Joshi, N. S. Saxena et al., *Bull. Mater. Sci.*, 26 (4) 387–389. (2003)

[57] R. A. Smith, *Semiconductors, second edition ed., Cambridge University Press: Cambridge,* 1978.

[58] Köseoğlu,Y., Alan, F., Tan M., Yilgin, R., Özturk M. Low temperature hydrothermal Synthesis and characterization of Mn doped cobalt ferrite Nanoparticles Ceramics International 38 3625-3634. (2012).,

[59] Yu,X.,Meng,D.,Liu,C.,He,X.,Wang,Y.,Xie J., ''Structure and ferromagnetism of Fe- doped and Fe-and Co-codoped ZnO nanoparticles synthesized by homogeneous precipitation method'' *Material letter* 86 112-114 (2012).

[60] Vidya, S., Baddhudus,R., ‘’Synthesis and magnetic behaviour of Mn:ZnO nanocrystalline powders’’ *Molecular and Biomolecular Spectroscopy Spectrochimica Acta Part A* 75 1218-1222 (2010).

[61] S. Kumar, R. Kumar, D. P. Singh, Appl. Surf. Sci. 255 8014-8018 (2009).

[62] M.K. Patra, K. Manzoor, M. Manoth, S. R. Vadera, N. Kumar, *Journal of Physics and Chemistry of solids*, 70 659-664 (2009).

[63] S. Benramache and B. Benhaoua, *Superlattices and Microstruct*., 52 1062-1070 (2012)

[64] Xue-Chao Liu, Er-Wei Shi, Zhi-Zhan Chen et al. *Journal of Crystal Growth* 296 (2006) 135-140.

[65] T.Wang et al. *Journal of Alloys and Compounds* 509 9116-9122. (2011).

[66] R.Al Asmar, G. Feblantier, J. L. Sauvajol, A. Giani, A. Khoury, A. Foucaran, *Microelectronics Journal* 36 (2005) 694-699.

[67] R. Pappalardo, D. l. Wood, R. C. Linares, *J. Chem.*, 35 (1991) 2041-2059.

[68] P. Koidl, *Phys. Rev.* B 15 (1977) 2493.

[69] Köseoğlu,Y.Alan Furkan a, Tan Muhammmed a, Yilgin Resul b, Özturk Mustafa *Ceramics International* 38 (2012) 3625-3634.

[70] Hao, Y.M., Lou, S., Zhou ,S., Wang, Y.,Chen,X., Zhu , G., Yuan, R., Li, N.,’’Novel magnetic behavior of Mn-doped ZnO hierarchical hollow spheres’’ *Journal Nanopart Res* 14:659 (2012).

[71] Rao C.N.R and Deepak F.L.,’’ Absence of ferromagnetism in Mn- and Co-doped ZnO’’ *chemistry and physics of materials units.* Bangalore 560064, India.

[72] Nguyen ,T ,Canhi, V., Dinh,T., Ngoc,N., Xuan, N., Nguyen,Q *journal of physics Conferences series* 187 (2009)012020.